

**Exploring the Controls on Marine Habitat Availability and Ecosystem
Function through Time with Idealized Model Worlds**

Sherry Yueh Xu

Faculty advisor: Pincelli Hull

Co-advisors: Andy Ridgwell and Dominik Hülse

Secondary reader: Derek Briggs

May 2, 2022

A Senior Thesis presented to the faculty of the Department of Earth and Planetary Sciences,
Yale University, in partial fulfillment of the Bachelor's Degree.

In presenting this thesis in partial fulfillment of the Bachelor's Degree from the Department of Earth and Planetary Sciences, Yale University, I agree that the department may make copies or post it on the departmental website so that others may better understand the undergraduate research of the department. I further agree that extensive copying of this thesis is allowable only for scholarly purposes. It is understood, however, that any copying or publication of this thesis for commercial purposes or financial gain is not allowed without my written consent.

Sherry Xu
May 2, 2022

Abstract

Major aspects of the Earth system, including climate, atmospheric oxygen, the strength of the biological pump, and export productivity from plankton communities, have varied dramatically through time. How these factors might have interacted to shape the evolution of marine life and ecosystems is not known. Here I apply the cGENIE Earth system model of intermediate complexity towards two areas of inquiry. First, I investigate how various tectonic and environmental factors interact to affect the availability of oxic benthic habitat, to consider how marine habitat availability may have changed since the rise of eukaryotes. I then investigate how evolutionary changes in plankton community size structure might have led to changes in surface export productivity, a major component of the marine carbon cycle, through time. Importantly, to address these questions, I develop and describe three idealized model worlds that are utilized in both investigations. These worlds simplify my exploration of various biotic and abiotic conditions throughout Earth history by representing some end members of tectonic change through time, and provide the additional advantage of being less computationally intensive to run than typical cGENIE configurations. I find that complex and nonlinear feedbacks dictate the availability of oxygenated habitat on the marine benthic shelf, and that larger plankton sizes through time generally drive a unidirectional trend of increased carbon export, except for in instances where evolution in zooplankton size lag behind evolution in phytoplankton size and then later catch up. The idealized model worlds presented here provide an empirical basis for addressing broader questions of how different Earth system states have impacted the history of life, and vice versa.

Table of Contents

Preface	5
Exploring the interacting effects of boundary conditions on benthic shelf oxygenation using model worlds	6
1.1 Introduction	6
1.2 Model description and method	8
1.2.1 Idealized continental configurations	9
1.2.2 Boundary condition experiments	10
1.2.3 Oxidic habitat availability analysis	11
1.3 Results	12
1.4 Discussion	13
1.4.1 Key controls on oxidic marine habitat availability	13
1.4.2 Complex and nonlinear feedbacks determine oxidic habitat availability in model worlds	15
1.4.3 From model worlds to history of marine life on Earth	18
1.5 Conclusion	20
1.6 Figures	22
Modeling the evolution of biological pump strength as a function of plankton community size structure	28
2.1 Introduction	28
2.2 Methods	30
2.2.1 Model description	30
2.2.2 Modeling plankton communities and tectonic settings	31
2.2.2 Note on terminology	32
2.3 Results	32
2.4 Discussion	33
2.4.1 Maximum plankton size in plankton communities affects broad patterns in carbon export	33
2.4.2 Grazing release from absence of large zooplankton can drive high carbon export	34
2.4.3 Implications for export productivity through time and the mediating influence of tectonics	35
2.5 Conclusion	36
2.6 Figures	38
Appendix 1	42
S1.1 Additional model information and references	42
S1.2 Diagnostic properties of model worlds at default environmental conditions	42
S1.2.1 Surface currents	42

	4
S1.2.2 Deep ocean flow	43
S1.2.3 Temperature and salinity	44
S1.2.4 Nutrients and productivity	45
S1.2.5 Ocean oxygen and euxinia	46
S1.2.6 Sea ice	47
S1.3. Additional description of isolated and combined effects of continental configuration, atmospheric $p\text{CO}_2$, atmospheric $p\text{O}_2$, and sinking rate on benthic shelf oxygenation	48
S1.3.1 Isolated effects of continental configuration on benthic shelf oxygenation	48
S1.3.2 Isolated effects of atmospheric $p\text{CO}_2$ on benthic shelf oxygenation	49
S1.3.3 Isolated effects of atmospheric $p\text{O}_2$ on benthic shelf oxygenation	49
S1.3.4 Isolated effects of sinking rate on benthic shelf oxygenation	50
S1.3.5 Combined effects of tectonic and environmental factors on fraction of anoxic benthic shelf area	50
Supplementary Table 1.1	52
Supplementary Figures 1.1 to 1.9	53
Appendix 2	63
S2.1 Possible correlation between plankton size and productivity	63
S2.2 Estimates of plankton size through time	64
S2.2.1 Scope and evidence	64
S2.3 Estimates of productivity through time	65
S2.3.1 Productivity estimates through time	65
S2.3.2 Export productivity and primary productivity	67
Supplementary Table 2.1	68
Supplementary Figures 2.1 to 2.2	73
Acknowledgements	75
References	76

Preface

I was lucky to be advised, mentored, and assisted by Pincelli Hull at Yale and Andy Ridgwell and Dominik Hülse at the University of California, Riverside, for the work that is presented in this thesis. This thesis centers around the application and analysis of three model worlds, with contrasting idealized continental configurations, using the Earth system model cGENIE. The two parts of this thesis both make use of these idealized model worlds but apply and analyze them with different motivations. Part one uses the model worlds to investigate tectonic and environmental influences on marine oxygenation and habitat availability; I began this project with Pincelli Hull, Andy Ridgwell, and Dominik Hülse in June 2019. Part two uses the model worlds to investigate how carbon export from plankton communities changes with community size structure and continental configuration; this work began in July 2021, again with Pincelli Hull, Andy Ridgwell, and Dominik Hülse.

This thesis is organized into two chapters with the main text and figures for each chapter presented in turn. Both chapters have supplemental material, including text, tables, and figures, which are provided in Appendix 1 and 2 respectively. A single reference section is provided and is included at the end of this document.

Exploring the interacting effects of boundary conditions on benthic shelf oxygenation using model worlds

1.1 Introduction

MacArthur & Wilson (1964) famously proposed that species richness should be positively related to habitat area and inversely related to the distance between habitat fragments in their theory of island biogeography. This simple mathematical framework has proven remarkably powerful for predicting diversity patterns today (e.g., Kreft et al. 2008; Tittensor et al. 2010; Jetz & Fine 2012). Paleontologists have long sought to apply such ecological rules to explain trends in the fossil record, including dramatic changes in marine diversity throughout the Phanerozoic (Sepkoski 1997). Studies to date have tested the effect of rock volume and area, sampling site area, sea area and sea level, coastline shape, and continental fragmentation and coalescence as possible factors that have driven changes in marine diversity over time (e.g., Raup 1976; Sepkoski 1976; Flessa & Sepkoski 1978; Valentine & Jablonski 1991; Barnosky et al. 2005; Holland 2012; Zaffos et al. 2018), based on the hypothesis that plate tectonics are a key regulator of ancient habitat availability (Valentine & Moores 1970; Bush & Payne 2021). Most have failed to find compelling evidence for habitat size and fragmentation in driving marine diversity patterns through the Phanerozoic.

However, habitat availability in the marine realm is not simply a matter of space. For metazoans, oxygen availability is a critical determinant of habitability but has been largely unexplored with regards to understanding marine habitat availability through time. Oxygen availability limits the range of many marine organisms and, in conjunction with temperature, is vital in meeting their metabolic demands, both today and in the geologic past (Deutsch et al.

2015; Deutsch et al. 2020; Boag et al. 2018; Hammarlund et al. 2017). The exclusion of this factor may account for the failure to find a correlation between habitat area and diversity in the fossil record.

Determining the spatial extent and connectedness of well-oxygenated marine habitat through time is complicated by the fact that multiple interacting factors determine oxygenation of the marine realm. This study focuses on four main factors—continental configuration, global temperature, atmospheric oxygenation, and the strength of the biological pump—which constitute tectonic and environmental controls on marine habitability. These factors are all known to affect ocean oxygenation and even each other (Lu et al. 2018; Stockey et al. 2021; Meyer et al. 2016; Reinhard & Planavsky 2021; Cole et al. 2021; Meyer & Kump 2008). Oxygenation of surface waters, for example, are not only dependent on atmospheric oxygen concentrations but are also mediated by ambient temperatures, which affect the solubility and bioavailability of oxygen in water (e.g., Boag et al. 2018). The decay, or remineralization, of organic matter sinking from the surface to the deep ocean is another major factor determining the availability of oxygen in underlying waters. The strength of this process, known as the biological pump, likely has changed through time due to the evolution of marine plankton and fluctuations in global temperature, given the temperature-dependence of microbial metabolisms (e.g., John et al. 2014). Meanwhile, changes in continental configuration modify ocean circulation patterns and, in turn, ocean ventilation, deep water aging, marine temperature, and mixed-layer nutrient availability—all of which ultimately shape the amount of distribution of oxygen in the ocean (e.g., Donnadieu et al. 2016; Friedrich et al. 2008).

Uncertainty surrounds the main influences on marine oxygenation over geologic time. Though we know that continental configuration, global temperature, atmospheric oxygenation,

and the strength of the biological pump have changed throughout time, owing to plate tectonics, volcanism, innovations in the biosphere, and other Earth system interactions and feedbacks, the exact timing and magnitude of these changes are still subjects of ongoing study. Thus a critical first step in investigating marine diversity through the lens of oxygenated habitat is to understand the sensitivity of benthic oxygenation to these four factors and their interactions. Here we utilize a model approach to evaluate the influence of these four factors on oxic habitat availability in the marine realm. We apply the cGENIE Earth system model configured in three contrasting idealized continental configurations to explore tectonic drivers of marine oxygenation and vary atmospheric CO₂, atmospheric O₂, and the sinking rate of particulate organic matter (and hence the strength of the biological pump) to assess the role of changing environmental boundary conditions. We describe the diagnostic properties of these three idealized worlds in a supplement and focus our main results on the spatial extent and fraction of oxygenated habitat on the benthic continental shelf, as relatively shallow marine environments like this one have been comparatively well-preserved through the Phanerozoic and shape our perception of the history of life (Shaw et al. 2020; Bottjer 2016). Our idealized model results provide an empirical basis for addressing broader questions of how different Earth system states vary in their habitability and overall suitability for marine life.

1.2 Model description and method

cGENIE consists of a 3-D frictional geostrophic ocean model with biogeochemical cycling, a 2-D atmosphere model with energy and moisture balance, and a dynamic-thermodynamic sea-ice model which also acts as a coupling module for the ocean and atmosphere components (Edwards and Marsh 2005; Marsh et al. 2011). As an Earth system

model of intermediate complexity, cGENIE captures major features of the living Earth system while requiring relatively low computational resources (Edwards and Marsh 2005; Marsh et al. 2011; Ridgwell et al. 2007). It has been tested extensively against modern observations of nutrients, oxygen, and the carbon cycle and employed in numerous studies of climate, biogeochemistry, and biological productivity over a range of time periods (e.g., Ridgwell & Schmidt 2010; Norris et al. 2013; John et al. 2014; Meyer et al. 2016; Lu et al. 2018; Reinhard et al. 2019; Stockey et al. 2021).

In this study, the model oceans are represented in a 36x36 equal-area grid of longitude and latitude and vertically in 16 logarithmically-scaled depth layers (see Section S1.1 of Appendix 1). Vertical/horizontal mixing, rather than isopycnal/diapycnal mixing, is used in order to simplify model calculations and minimize the occurrence of negative tracer values in the ocean (see Section S1.1 of Appendix 1). The model is climate-sensitive (5.77 W/m² radiative forcing per doubling of CO₂), with temperature-dependent remineralization rates for sinking organic matter after Crichton et al. (2021). Components of the marine biological pump are otherwise defined after Ward et al. (2018) with PO₄ and Fe co-limitation of biological productivity and a marine iron cycle. All worlds are initialized with modern default values for solar luminosity (1368 W/m²), mean ocean salinity (33.9 PSU), and dissolved sulfate inventory (29.16 mmol/kg). Biological new production is set by the half-saturation constant of PO₄ (0.1 μmol/kg), half-saturation value of Fe (0.1 nmol/kg), and timescale of biological uptake (63.38 days). Albedo is prescribed according to Supplementary Figure 1.1a and an intermediate zonal wind stress field is applied according to Supplementary Figure 1.1b.

1.2.1 Idealized continental configurations

We configure the Earth system model cGenIE in three different idealized continental configurations, which we refer to as the ‘block’ world, ‘equator’ world, and ‘polar’ world. Each world features an ocean with a single, large continent in a specific orientation meant to represent a few end-member tectonic configurations with regards to their effect on ocean circulation (Figure 1.1). In the block world, the continent stretches from pole to pole across all latitudes. In the equator world, the continent covers only low latitudes and features an equatorial gateway. In the polar world, the continent covers only high latitudes, centered on the North pole. The continent in each world is surrounded on all sides by a continental shelf that steps down in four depth-steps of 81 m, 284 m, 558 m, and 928 m. The ocean floor is 3576 m deep. Ocean volumes in each world are roughly equal and listed in Supplementary Table 1.1 along with ocean surface area, average ocean temperature, ocean O₂ concentration, ocean PO₄ concentration, and total POC export. Diagnostic properties of these worlds are presented in Figure 1.2 (focusing on baseline ocean oxygenation) and Section S1.2 of Appendix 1 (describing surface currents, deep ocean flow, temperature and salinity, nutrients and productivity, ocean oxygen and euxinia, and sea ice). We have included the cGenIE representation of the modern world, with a modern continental configuration (after Crichton et al. 2020), in Figures 1.1 to 1.2 and Supplementary Figures 1.2 to 1.4 to provide a direct comparison of the various physical and biogeochemical attributes of the three idealized model worlds to the world as it is known today.

1.2.2 Boundary condition experiments

For each of the three idealized continental configurations, we initialized a series of cGenIE model simulations with different atmospheric pCO₂ levels, atmospheric pO₂ levels, and

organic matter sinking rates to test how these factors interact to affect benthic oxygenation on the continental shelf. We focus our analysis on the continental shelf as this is the marine environment best preserved in the fossil record through the Phanerozoic and older strata. Atmospheric $p\text{CO}_2$ is included as a forcing on global temperature, and we set atmospheric $p\text{CO}_2$ to 1, 2, 4, or 8 times that of the modern pre-industrial value (278 ppm). Atmospheric $p\text{O}_2$ is set to 0.2, 0.3, 0.4, 0.5, 0.75, or 1 times that of present (1 PAL, or 209,500 ppm). Organic matter sinking rate is varied to simulate changes in the biological pump strength, with a faster sinking rate resulting in a more effective transport of organic matter from the surface to deep ocean (e.g., a stronger biological pump). Organic matter sinking rates are set to 0.2, 0.4, 0.6, 0.8, or 1 times that of the modern value (125 m/day). In total, we test 360 parameter combinations, with 120 combinations of environmental conditions for each of our three continental configurations. Each parameterized model world is spun up for 10,000 years to allow equilibrium to be reached before we assess the effect of these various environmental and tectonic boundary conditions on benthic oxygenation. Modern-like conditions of 1x $p\text{CO}_2$, 1x $p\text{O}_2$, and 1x sinking rate serve as our default environmental boundary conditions.

1.2.3 Oxic habitat availability analysis

We present results on how our parameterizations of tectonic and environmental factors (i.e., continental configuration, atmospheric $p\text{CO}_2$ levels, atmospheric $p\text{O}_2$ levels, and sinking rates of organic matter) influence the fraction of anoxic area on the benthic continental shelf in each of the 360 cGENIE model simulations described above. We define anoxic conditions as any dissolved O_2 concentration below 5 $\mu\text{mol O}_2/\text{kg}$. Other thresholds for anoxia, based on Sperling et al. (2013), were also tested, with no significant change in results (Supplementary Figure 1.5).

Since each grid cell in the cGenIE model represents an equal amount of surface area (Edwards & Marsh 2005; Marsh et al. 2011), we simply calculate the percentage of shelf cells with anoxic conditions relative to all shelf cells.

1.3 Results

Atmospheric pO_2 constitutes the single most influential control on the fraction of anoxic area on the benthic continental shelf (Figure 1.3). While atmospheric pCO_2 and sinking rate drives changes of <10% in available habitat area on the shelf over the range of values tested (Figure 1.3), variation in atmospheric pO_2 drives changes in available habitat area of >80%. In a fully oxygenated world (100% PAL, as represented in Figures 1.3a and 1.3c), variation in atmospheric pCO_2 and sinking rate ultimately have a minor influence on the fraction of anoxic benthic shelf area. Anoxic areas always remain under 10% of the total benthic shelf habitat. After atmospheric pO_2 , continental configuration has the next most pronounced effect on influencing the fraction of anoxic benthic shelf area. Different continental configurations, holding all other factors constant, can cause changes in % benthic anoxia that are at times greater in magnitude than the changes caused by variations in atmospheric pCO_2 and sinking rate alone (Figure 1.3).

Continental configuration is also notable because it modifies when and to what degree a change in atmospheric pO_2 (and other environmental factors) affects benthic anoxia. For example, 50% PAL is a crucial inflection point for the block world, below which benthic anoxia becomes far more pervasive on the continental shelf (Figure 1.3b). However, this number is 75% PAL for the equator world and 40% PAL for the polar world (Figure 1.3b). Complete results from all 360 model simulations, regarding the interactive effects of continental configuration,

atmospheric $p\text{CO}_2$, atmospheric $p\text{O}_2$, and sinking rate on oxygenation of the benthic shelf, are shown in Figure 1.4 and discussed below. Further description of both the individual and combined effects of continental configuration, atmospheric $p\text{CO}_2$, atmospheric $p\text{O}_2$, and sinking rate on benthic shelf oxygenation can be found in Section S1.3 of Appendix 1.

1.4 Discussion

1.4.1 Key controls on oxic marine habitat availability

For most of the history of life, the marine realm was characterized by far lower oxygenation saturation states than the present day (Lu et al. 2018). Geochemical and sedimentological evidence suggest that widespread anoxia was common through the Paleozoic and much of the Mesozoic, lagging behind the oxygenation of the atmosphere. The prolonged presence of widespread anoxia in the marine realm has important implications for understanding the evolution and ecology of marine ecosystems because the vast majority of metazoans require some level of oxygenation to live, although the exact amount varies amongst species and clades. Thus, a first order effect of prolonged widespread marine anoxia would be the reduction of the amount of habitat available for metazoans. Such reductions in habitat availability pose direct implications for the diversity and longevity of marine species through time.

Important though this may be, understanding and predicting exactly how much—and at what depths—oxygenated marine habitat has been available through time is complicated, because numerous factors can interact to modulate marine oxygenation. Within our idealized model worlds (Figure 1.1), we find that atmospheric oxygenation and continental configuration are the two most important factors constraining the range and extent of anoxia in benthic marine environments and, therefore, the extent of habitable benthic marine environments. In this study,

we focus on relatively shallow, benthic habitats as they reflect the environments best preserved in the marine fossil record and, by extension, the region responsible for our understanding of diversity dynamics through time.

Atmospheric pO_2 is the most influential factor controlling the extent of anoxia on the benthic continental shelf (Figure 1.3; Figure 1.4). Across all tectonic and environmental configurations, one broad trend holds true: higher pO_2 helps to minimize anoxic conditions on the benthic shelf. pO_2 conditions of 75 to 100% PAL, for example, can maintain fractions of anoxic benthic shelf area under ~50% in all worlds, regardless of the status of other environmental conditions such as pCO_2 and sinking rate (Figure 1.4a, b, c).

Continental configuration is the next most influential control. In our simulations, the block world experiences ~5 to 80% anoxia on the continental shelf across all environmental conditions (Figure 1.4a), as compared to ~20 to 100% anoxia in the equator world and 0 to 100% the polar world. Thus a world's tectonic configuration can set upper and lower bounds on the range of benthic shelf anoxia that organisms experience, even as other environmental factors change. Indeed, the placement of continents is known to influence factors like circulation, upwelling, and local productivity, which all can contribute to the regulation of the amount and spatial extent of marine oxygenation. Our model worlds additionally show that continental configuration can influence the rate at which the Earth system shifts from one biogeochemical state to another. In other words, the sensitivity of benthic shelf oxygenation to changes in atmospheric oxygenation, climate, and the biological pump depends on continental configuration. The transition from minimally anoxic to highly anoxic shelves in the block world are always relatively gradual in response to changes in pO_2 , temperature (modeled via pCO_2), and the strength of the biological pump (i.e., sinking rate) (Figure 1.4d, g, j, m, p), in contrast to

more abrupt transitions in the equator world (Figure 1.4e, h, k, n, q) and polar world (Figure 1.4f, i, l, o, r) especially when both pO_2 and sinking rates are low.

1.4.2 Complex and nonlinear feedbacks determine oxic habitat availability in model worlds

Though the impact of atmospheric pO_2 and continental configuration on benthic shelf oxygenation is particularly evident in our model worlds, all four factors investigated influence the magnitude and extent of oxygenation in the marine realm. For example, model simulations with relatively high biological pump strength (i.e., relatively high sinking rates) generally correspond to more extensive benthic anoxia on the shelf (e.g., Figure 1.4d, e, f, g, h, i, j, k, l). More importantly, however, we find strong evidence for pronounced, nonlinear interactions amongst the four factors (Figure 1.4), particularly in the equator and polar worlds (e.g., see Figure 1.4b, c, e, f, i, l, especially in contrast to Figure 1.4a).

We focus our discussion of nonlinear interactions on how global temperatures (regulated by our parameterization of pCO_2) affect oxic habitat availability on the benthic shelf; the directionality of the effect of pCO_2 changes based on how sinking rates are parameterized. In the block world, lower pCO_2 settings reduce the spatial extent of anoxia, all other factors held constant, for the 0.2x sinking rate biological pump strength scenario (Figure 1.4p), but these lower pCO_2 settings instead increase shelf anoxia when sinking rates are high (0.4x, 0.6x, 0.8x, and 1x sinking rate, Figure 1.4m, j, g, d). This pattern is true for other worlds as well, though exact points of transition differ. For example, lower pCO_2 settings reduce anoxia at 0.2x and 0.4x modern sinking rates in the equator and polar worlds (Figure 1.4q, n and Figure 1.4r, o), but increase anoxia at higher sinking rates (0.6x, 0.8x, and 1x, Figure 1.4k, h, e and Figure 1.4l, i, f). The interactions of these parameters are even more complex in the equator and polar worlds at

1x sinking rate (Figure 1.4e, f).

Why do such points of transition, relating to the interplay of temperature (regulated by $p\text{CO}_2$ and sinking rate, appear in our model worlds? To explain these points of transition, we first propose that two main controls on oxygenation of the water column exist: (1) the rate at which organic matter is remineralized as it passes through the water column, and (2) the solubility of O_2 in the water. Remineralization rates are determined by both sinking rate and temperature: sinking rate dictates *how much* organic matter is present in any given layer of the water column that is *available* to be remineralized (e.g., if there is no organic matter in a given layer of the water column, remineralization simply will not occur); and temperature dictates the *speed* at which remineralization of available organic matter occurs, since remineralization rates are temperature-dependent and increasing with higher temperatures. The solubility of O_2 is determined by temperature alone, increasing with colder temperatures. While both these controls influence water column oxygenation, we hypothesize that remineralization rates are more influential when there is *ample* organic matter in the water column available for remineralization, and solubility effects are more influential when there is *minimal* organic matter sinking through the water column.

Next we turn to our model results to illustrate the interplay of these effects. When sinking rates are low (25 m/day, or 0.2x of modern - Figure 1.4p, q, r), organic matter is suspended for longer periods of time in the surface layer of the ocean, such that the vast majority of it is respired there (Figure 1.5b). This is the case regardless of temperature effects on remineralization, as even the slowest effective remineralization rates in the 1x $p\text{CO}_2$ scenario still result in nearly all organic matter being remineralized in the surface layer; this is evident from the sharp decreases in surface-layer oxygen that can be seen across all $p\text{CO}_2$ scenarios (Figure

1.5b). Thus, minimal amounts of organic matter remain available to sink to lower depths of the water column, and at these lower depths, solubility of O_2 becomes more influential than remineralization rates in determining water column oxygenation. In lower sinking rate scenarios, lower pCO_2 conditions help to reduce benthic anoxia on the shelf, all other factors held constant, because they increase the solubility of O_2 at subsurface layers of the water column.

On the other hand, when sinking rates are high (Figure 1.4d, e, f), more organic matter makes it past the surface layer to greater depths of the ocean, even when remineralization rates are highest in the 8x pCO_2 scenario (Figure 1.5a). Thus, because there is ample organic matter to be remineralized at every layer of the water column, remineralization rates are more influential than O_2 solubility in determining water column oxygenation. Lower pCO_2 conditions result in lower remineralization rates, and here the effect of lower remineralization rates is twofold: (1) lower remineralization rates within one layer of the water column help to decrease oxygen demand in that particular layer of the water column; (2) lower remineralization rates mean that more organic matter remains at a certain layer of the water column, which means that more organic matter is available to be exported to lower layers of the water column. We argue that this second effect of lower remineralization, taking the dynamics of organic matter moving throughout the whole water column into account, is most important: effectively, lower remineralization rates lead to a greater overall amount of organic matter that stays suspended in the water column. All of this organic matter, then, is subject to remineralization, and more *total* remineralization occurs throughout the whole water column, even though remineralization *rates* are lower. Thus, in higher sinking rate scenarios, lower pCO_2 conditions increase benthic anoxia on the shelf, all other factors held constant, because they increase the sum total amount of organic matter that is subject to remineralization throughout the entire water column.

Finally, we note that points of transition in how $p\text{CO}_2$ and sinking rate interact to affect benthic shelf oxygenation rely on not only the distribution of organic matter through the water column and solubility of O_2 in water, but also the configuration and depth of the continental shelf area. In the case of lower sinking rates and lower $p\text{CO}_2$ especially, the model shelf (which comprises 4 steps at 81 m, 283 m, 558 m, and 928 m) is able to benefit from the minimal amounts of organic matter in subsurface layers because the majority of it exists below ~ 100 m. For example, if our model worlds had shallow continental shelves only 50 to 100 m deep, it is doubtful that points of transition would be observed, as key differences in water column oxygenation are only present below ~ 100 m in our O_2 depth profiles (Figure 1.5).

1.4.3 From model worlds to history of marine life on Earth

The model worlds and scenarios used here are highly simplified compared to conditions that existed during the evolution of life on earth, yet they are useful for considering how marine oxygenation would have varied in response to evolving environmental conditions. Several lessons emerge from these models:

1. ***Oxic habitat availability likely fluctuated in response to factors beyond atmospheric $p\text{O}_2$ for much of the Phanerozoic.*** Long after significant oxygenation of the atmosphere, the majority of the deep sea remained anoxic (Sperling et al. 2015, Lu et al. 2018) and prone to periods of extensive global anoxia (e.g., Jenkyns 2010). Our modeling shows that all the environmental and tectonic factors considered here can interact nonlinearly to drive extensive anoxia. In our model worlds, continental configuration is by far the strongest of the levers, after atmospheric $p\text{O}_2$, in controlling the oxygenation of the shelf. However, we note that the dominance of this factor may be specific to our modeled

worlds because the simplified continental and ocean configuration results in an overly deep mixed layer relative to the world as we know it (Figure 1.1d; Supplementary Figure 1.2; see Section S1.2.1 and S1.2.2 of Appendix 1). This has cascading effects, including supporting extremely productive upwelling zones and extensive oxygen minimum zones. In other words, the idealized configurations of our model worlds exert a strong physical control on the intensity and spatial extent of marine anoxia—both of which are likely stronger than what has occurred in the real world under similar atmospheric O₂ conditions. Even so, the nonlinearity of tectonic and environmental interactions, and the effect of these interactions (e.g., producing inflection points in anoxia with directional changes in underlying factors, as discussed above with $p\text{CO}_2$ and sinking rate), are likely a robust finding.

2. ***Evolution of plankton ecosystems may have led to increased or decreased shelf***

oxygenation depending on environmental and tectonic conditions at the time. This is arguably the most important and surprising finding of our results. The evolution of larger plankton and more complex plankton ecosystems is generally supposed to have increased the ability of biological pump to export carbon to the deep ocean, consequently shifting the nexus of organic matter remineralization from the shallow to deep ocean leading to greater oxygenation of shelf environments. Here our model results show that this shift in remineralization does indeed impact mid-water oxygenation, but whether this increases or decreases oxygenation of shelf environments is strongly dependent on the initial conditions and depth of the shelf. Additionally, given the interactions of sinking rate and atmospheric $p\text{CO}_2$ in driving shelf oxygenation, it is also possible to imagine a scenario where the effect of biological evolution on biological pump efficiency is neutralized or

reversed by global temperatures.

3. ***The rate of change in tectonic and environmental factors can influence the rate of change in ocean anoxia.*** Some of the factors investigated, like continental configuration, change more slowly through time than others like temperature or biological pump strength. We therefore predict a relationship between the magnitude and rate of change in benthic shelf anoxia and the underlying frequency of tectonic and environmental change.
4. ***Complex dynamics in the extent and variability in benthic habitat availability can arise from the interaction of relatively few factors.*** Returning to the motivating question of this research, we suspect that the true availability of benthic marine habitat throughout the Phanerozoic was likely as much controlled by the extent and stability of benthic shelf oxygenation as it was by other factors considered to date like shelf area, continental fragmentation, and sea level. Evidence for extensive marine anoxia through much of the Phanerozoic, in conjunction with the late rise of marine diversity towards present-day levels, supports this idea that the *oxygenation* of available habitat could be a crucial factor controlling the spatial extent and distribution of benthic habitat through time.

1.5 Conclusion

The goal of this current investigation is to explore how different abiotic and biotic factors may have interacted over the Phanerozoic using highly idealized model worlds, in order to provide a foundation for understanding the relative impact and feedbacks of such factors in driving benthic marine habitat availability, particularly oxygenated habitat availability. Over the history of life, continental configuration, atmospheric $p\text{CO}_2$, atmospheric $p\text{O}_2$, and the strength of the biological pump have all changed, but two are most important for maintaining available

oxygenated habitat: atmospheric pO_2 and continental configuration. Continental configuration changes the amount of oxic habitats, all else being the same, but its relationship to marine habitat availability is not a simple matter of coastline length or ocean area. Instead, continental configuration sets bounds on the extent and location of marine upwelling relative to benthic shelves, and the recycling and export of organic matter. While atmospheric pO_2 and continental configuration place key constraints on the patterns of anoxia on the shelf, other factors such as global temperature and biological pump efficiency also alter and mediate the extent of ocean anoxia (and thus, oxic habitat availability through time) in important, nonlinear ways.

Our idealized worlds provide a fast interactive framework for investigating the effect of various tectonic and environmental factors on marine ecosystems through time. These simple, idealized model worlds provide a means of considering the complex interplay of abiotic and biotic factors in Earth history, and set up a framework for testing complex Earth system interactions across a wide array of problems.

1.6 Figures

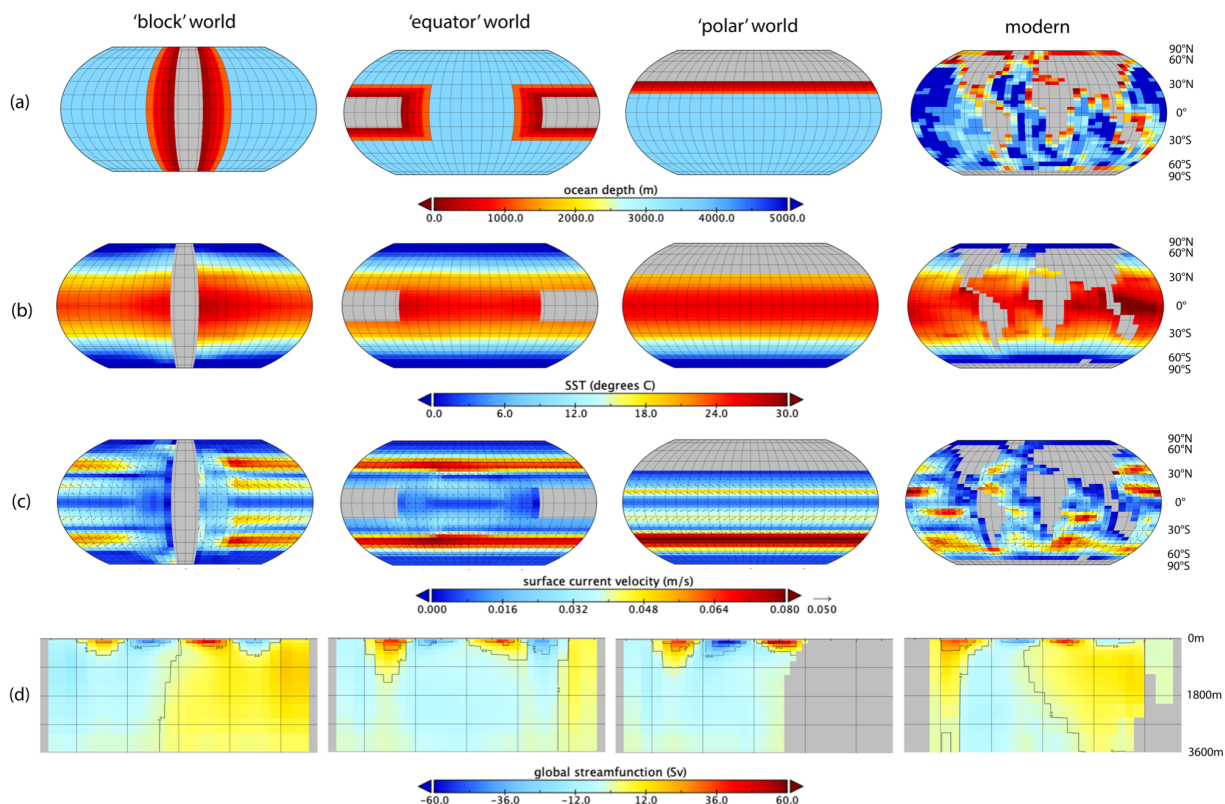


Figure 1.1: Bathymetry, SST, surface current field, and overturning circulation for each idealized continental configuration at default environmental conditions (i.e., pre-industrial modern $p\text{CO}_2$ at 228 ppm, modern $p\text{O}_2$ at 100% PAL, and modern sinking rate at 125 m/day), with modern world for comparison. (a)-(c) Vertical gridlines mark longitude in increments of 15 E-W and horizontal gridlines mark latitude in increments of 15 N-S. (d) Vertical gridlines mark latitude in increments of 30° N-S and horizontal gridlines mark depth in increments of 833 m from the surface.

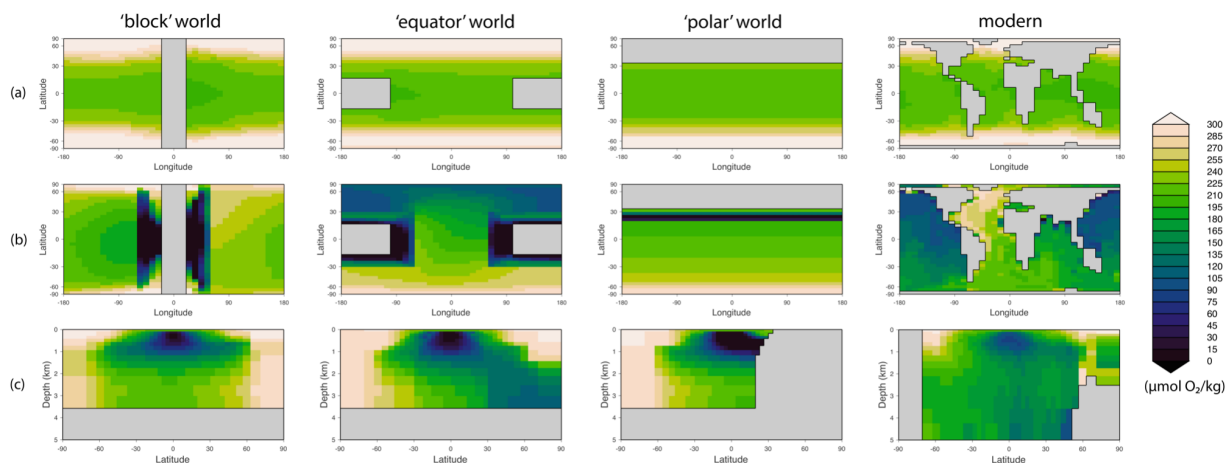


Figure 1.2: Ocean O₂ concentrations for each idealized continental configuration at default environmental conditions (i.e., pre-industrial modern $p\text{CO}_2$ at 228 ppm, modern $p\text{O}_2$ at 100% PAL, and modern sinking rate at 125 m/day), with modern world for comparison. (a) shows the surface ocean (longitude on x-axis, latitude on y-axis), (b) shows the benthic surface of the ocean (longitude on x-axis, latitude on y-axis), and (c) shows a vertical slice of the world (latitude on x-axis, depth on y-axis), with values averaged across longitudes.

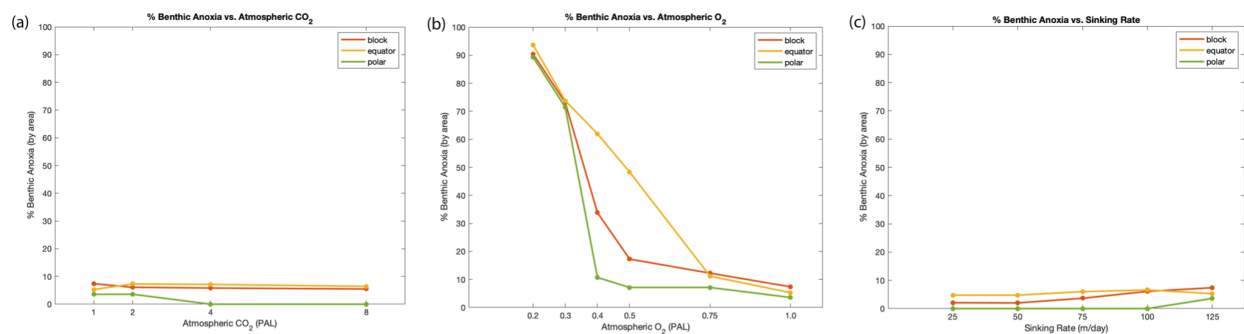


Figure 1.3: Isolated effects of (a) atmospheric pCO_2 , (b) atmospheric pO_2 , and (c) sinking rate on the fraction of anoxic area on the benthic continental shelf in each idealized world. For each graph, only continental configuration and the indicated variable are altered; all other factors are kept constant at default environmental conditions (i.e., pre-industrial modern pCO_2 at 228 ppm, modern pO_2 at 100% PAL, and modern sinking rate at 125 m/day). Anoxia is defined as oxygen concentrations below 5 $\mu\text{mol/kg}$.

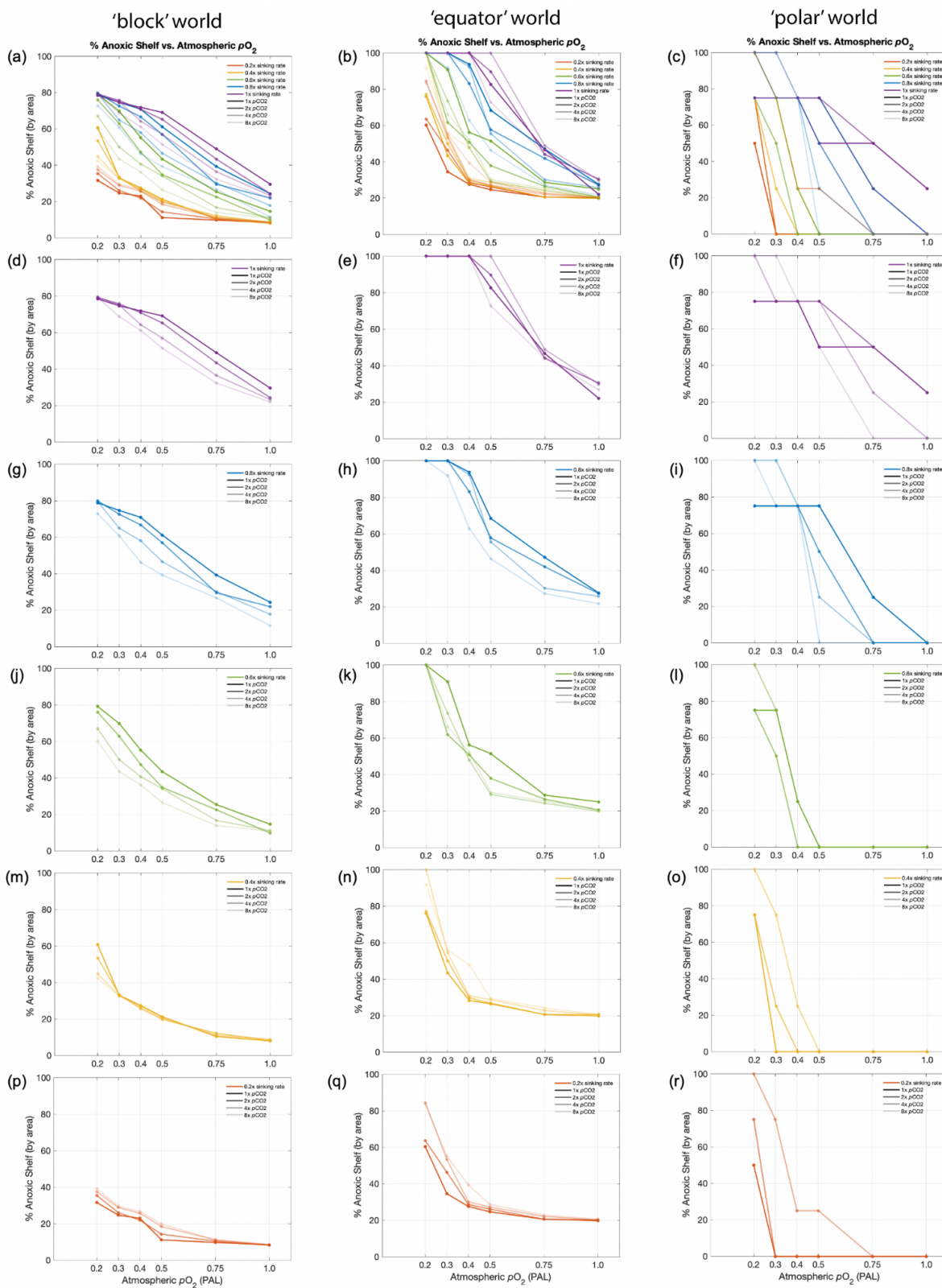


Figure 1.4: Fraction of anoxic area on the benthic continental shelf for all tectonic and environmental configurations of each idealized world. Each point on these plots represents a

single model experiment. Its x-coordinate indicates the atmospheric pO_2 setting; its color indicates the sinking rate setting (purple - 1x sinking rate (125 m/day, or modern), blue - 0.8x sinking rate (100 m/day), green - 0.6x sinking rate (75 m/day), yellow - 0.4x sinking rate (50 m/day), red - 0.2x sinking rate (25 m/day)); and its transparency or relative saturation indicates the atmospheric pCO_2 setting (full saturation - 1x pCO_2 (228 ppm, or pre-industrial modern), 2nd most saturated - 2x pCO_2 (556 ppm), 2nd least saturated - 4x pCO_2 (1112 ppm), least saturation - 8x pCO_2 (2224 ppm)). Its continental configuration is indicated by what column the plot is in (left to right - 'block' world, 'equator' world, and 'polar' world). Points that represent model experiments conducted at the same sinking rate setting (i.e., united by color) and the same atmospheric pCO_2 setting (i.e., united by relative saturation) are connected with a line. Finally, the y-coordinate of each point indicates the % area of benthic continental shelf that is anoxic ($< 5 \mu\text{mol/kg}$) in the model ocean of that particular model experiment. (a)-(c) show all 360 model experiments in one row, separated by continental configuration. For more convenient viewing, (d)-(f) only show model experiments at 1x sinking rate; (g)-(i) only at 0.8x sinking rate; (j)-(l) only at 0.6x sinking rate; (m)-(o) only at 0.4x sinking rate; and (p)-(r) only at 0.2x sinking rate. Additionally, (d)-(r) show gridlines for both axes.

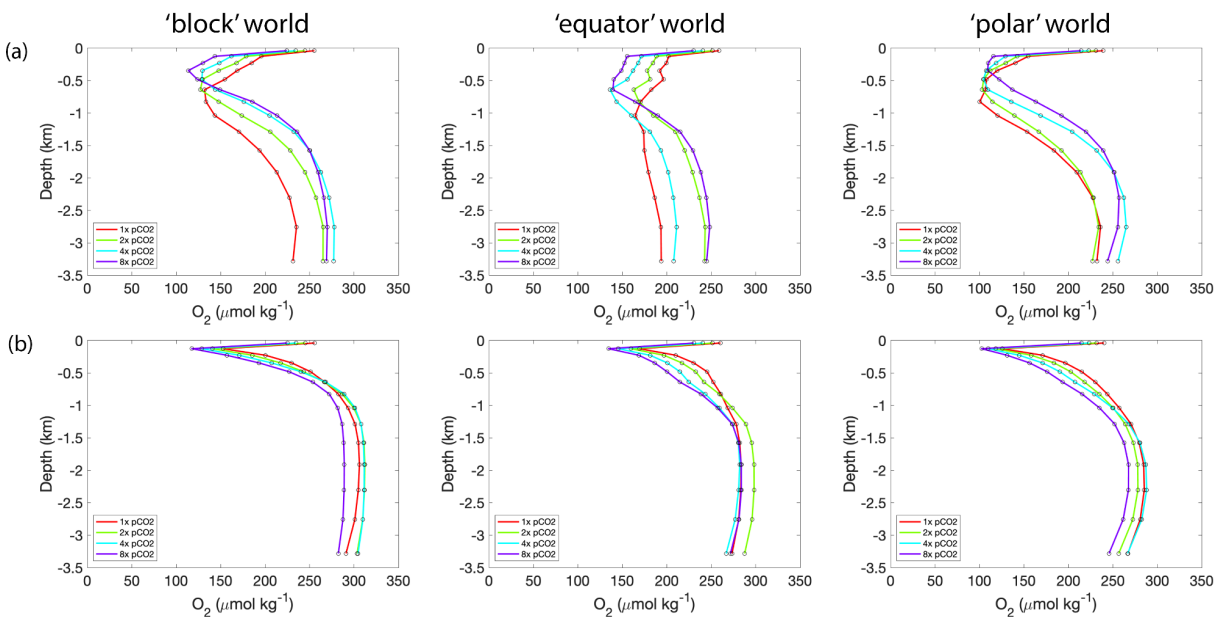


Figure 1.5: Depth profiles of marine O_2 in each world, at differing $p\text{CO}_2$ and sinking rate conditions, with constant $p\text{O}_2$ (100% PAL). Different $p\text{CO}_2$ conditions are marked by different colors according to the legend. (a) shows worlds at 1x sinking rate (125 m/day, or modern). (b) shows worlds at 0.2x sinking rate (25 m/day).

Modeling the evolution of biological pump strength as a function of plankton community size structure

2.1 Introduction

In the open ocean, a vast realm covering roughly seventy percent of the earth's surface, plankton communities make up much of the food web and perform a myriad of functions for marine ecosystems. At the base of the food web are phytoplankton, ranging in size and complexity from the micron-size bacteria plankton to the vast millimeter-long colonies of eukaryotic algae like diatoms or free-floating seaweed like *Sargassum*. These phytoplankton are eaten in turn by a range of predators, again ranging in size and complexity from bacteria and single-celled eukaryotes to relatively vast metazoans including larvaceans and whales. The importance of plankton communities to the Earth system is hard to overstate. The global primary productivity of marine phytoplankton is comparable to that of land plants (Field et al. 1998), and the structure and function of pelagic communities regulates the marine and global carbon cycle through the export and burial of carbon and key minerals (calcium carbonate and silica) from the surface ocean into geological archives (Falkowski et al. 2003). Carbon cycling in the ocean in turn affects factors like marine oxygenation and nutrient cycles, and even global temperatures. Innovations in phytoplankton and zooplankton have been linked to some major events in Earth history, including the Great Oxidation Event (Hurley et al. 2021), the Cambrian explosion (Butterfield 1997), and the Marine Mesozoic Revolution (Knoll & Follows 2016). Plankton communities as a whole have the capacity to exert considerable influence over the arc of primary productivity and export productivity through time (Figure 2.1; see also Section S2.1 in Appendix 2).

Modern pelagic ecosystems can be effectively modeled with a handful of functional traits, including plankton size and feeding ecology in nutrient-phytoplankton-zooplankton (NPZ) models of varying complexity (e.g., Follows et al. 2007). Trait-based models of plankton communities are increasingly employed in investigating the role of plankton in past Earth environments where the exact components of plankton diversity are unconstrained (Barton et al. 2013; Ward et al. 2018). Of all functional traits, size is particularly instrumental. It affects an organism's metabolism, nutrient requirements, nutrient uptake, prey selection, and more (Finkel 2007; Barton et al. 2013; Ward et al. 2018). Size—and size *structure*—can also determine the organic matter flux from a plankton community, though the relative contributions of differently sized plankton are debated (Guidi et al. 2009; Ward & Follows 2016; Planavsky et al. 2021). Plankton size therefore not only influences an individual organism's physiology but also higher-level characteristics such as trophic and competitive interactions with other plankton, a population's viability within the ecosystem, overall plankton community structure, and important community functions like carbon export and primary production (Finkel 2007; Guidi et al. 2009; Barton et al. 2013; Ward et al. 2018).

The size structure of pelagic communities has evolved markedly since plankton first appeared in Archean (Fig. 2.1a). Here, we investigate how changes in the maximum size of plankton in plankton communities affects the amount of carbon exported from the surface ocean, also known as the strength of the biological pump. Particularly we examine such changes relative to variations in continental configuration, and present some insights into the mechanisms that may have linked plankton size evolution with fluctuations in productivity and the carbon cycle through time.

2.2 Methods

2.2.1 Model description

We employ the cGenIE Earth model of intermediate complexity (Edwards and Marsh 2005; Marsh et al. 2011). cGenIE is configured as presented in Section 1.2 of this paper, with a gridded model ocean (Figure 2.2a) and PO_4 and Fe limitation of biological productivity, though there are two differences. First, temperature-dependent remineralization is not employed, as we do not test worlds with different $p\text{CO}_2$ levels in this study. Remineralization rates are solely depth-dependent after Ridgwell et al. (2007). Second, we apply ECOGEM, an ecological model component, to cGenIE (Ward et al. 2018); this combination of ECOGEM and cGenIE is referred to as EcoGenIE. In the default cGenIE, inorganic nutrients in the surface ocean are immediately converted to exported nutrients (particulate organic matter, POM) or dissolved organic matter (DOM) according to a preset partitioning scheme. EcoGenIE, on the other hand, allows for the resolution of a biological plankton community that exists in the surface layer of the model ocean (above ~ 80 m), and surface inorganic nutrients must pass through this plankton community before being converted to nutrients that will be exported from the surface layer (POM) or DOM (Ward et al. 2018).

Different populations of plankton within the community are parameterized according to plankton size and plankton functional type. In our configuration of EcoGenIE we utilize 2 possible functional types (“phytoplankton” or “zooplankton”) of plankton and 8 possible size classes (equivalent spherical diameter of 0.6 μm , 1.9 μm , 6 μm , 19 μm , 60 μm , 200 μm , 600 μm , or 2000 μm) (Figure 2.2a). Both “phytoplankton” and “zooplankton” are subject to nutrient requirements, mortality, and internal trophic interactions, but phytoplankton can only acquire nutrients through photosynthesis, and zooplankton can only acquire nutrients through feeding on

phytoplankton and other zooplankton (Ward et al. 2018). A plankton's size determines factors such as nutrient affinity, maximum photosynthetic rate, cell carbon quota, maximum prey ingestion rate, palatability as prey, and the partitioning of organic matter into exported nutrients (POM) and DOM after inorganic nutrients have been passed through the dynamic and explicit plankton community (Wilson et al. 2018; Ward et al. 2018). A full description of EcoGENIE can be found in Ward et al. (2018) and additional description in Wilson et al. (2018). We note that our configuration of EcoGENIE does not model mixotrophic-type plankton nor size-dependent sinking rates of organic matter in the water column, though such elements have been the subject of other investigations of plankton through time (e.g., Ward & Follows 2016; Knoll & Follows 2016). It also does not model any organisms below the surface layer (~80 m) nor any planktic organisms with sizes above 1900 μm .

2.2.2 Modeling plankton communities and tectonic settings

We run a suite of model experiments to capture the full range of possible maximum size classes of phytoplankton and zooplankton. Given our configuration of EcoGENIE, there are 8 possible maximum size classes for the phytoplankton and 8 possible maximum size classes for the zooplankton. This results in a total of 64 possible plankton community configurations (e.g., all 8 phytoplankton and all 8 zooplankton size classes are parameterized, or only the smallest 7 phytoplankton and all 8 zooplankton size classes are parameterized, and so on).

As for tectonic configurations, we do not aim to mimic the exact continental configurations found on Earth throughout time. Instead we employ 3 idealized model worlds meant to represent some end members of tectonic change (Figure 2.2b), each with one supercontinent either stretching from the North pole to the South pole ('block' world), positioned

on the equator with an equatorial passage ('equator' world), or centered on the north pole ('polar' world). Each supercontinent is surrounded on all sides by a continental shelf consisting of four steps and an ocean (of comparable volume among all three worlds). These model worlds and their diagnostic properties are described in Section 1.2.1 of this paper, and we use them here with no change.

The 64 possible plankton community configurations, applied to 3 possible tectonic configurations, result in a total of 192 distinct model simulations. We observe the amount of particulate organic carbon (POC) that is exported from the plankton community in the surface layer of the model ocean (0 to ~80 m) to the next deepest layer of the model ocean (~81 to ~175 m).

2.2.2 Note on terminology

We use the term "phytoplankton" to refer to any autotrophic planktic organisms that fix carbon through oxygenic photosynthesis (e.g., cyanobacteria and algae). "Zooplankton" is not limited to animals and instead refers to any heterotrophic planktic organism, or any planktic organism that may be thought of as autotrophic (i.e., self-reliant for nutritive organic substances) but does not fix carbon through oxygenic photosynthesis (e.g., planktic prokaryotes and copepods).

2.3 Results

Global mean of particulate organic carbon (POC) export varies with different maximum size classes of phytoplankton and zooplankton in all 3 idealized model worlds; such patterns are complemented by similar variations in mean PO_4 concentrations in the surface ocean, mean Fe

concentrations in the surface ocean, and global mean O₂ concentrations (Figure 2.2). These patterns are delineated and discussed below.

2.4 Discussion

2.4.1 Maximum plankton size in plankton communities affects broad patterns in carbon export

Two broad patterns can be observed in how the size structure of a plankton community (particularly in regards to its maximum plankton size among either phytoplankton or zooplankton) affects carbon export from the community. First, carbon export generally increases with size (Figure 2.2); in each plot of POC export among all three worlds, moving diagonally from the bottom left corner (representing the smallest phytoplankton and zooplankton) to the upper right corner (representing the full range of smallest to largest phytoplankton and zooplankton) results in increased carbon export. Second, carbon export is highest in each world when phytoplankton are larger and zooplankton are smaller (i.e., the bottom right corner of each plot of POC export).

These patterns are found in all three idealized model worlds, suggesting their robustness; the idealized model worlds instead differ in the absolute amount of carbon export that result from different plankton community size structures. For example, the block world is prone to higher amounts of carbon export (indicated by the swath of light yellow in the bottom left of the plot, as well as the overall lighter color gradients), followed by the equator world and then the polar world (Figure 2.2).

Changes in POC export in our model worlds are correlated with similar gradients of mean PO₄ concentrations in the surface ocean, mean Fe concentrations in the surface ocean, and global mean O₂ concentrations (Figure 2.2). These tandem changes are reasonable and point to possible

mechanisms for changes in POC export as well as ocean oxygenation. Decreased PO_4 and Fe in the surface ocean indicate higher nutrient uptake by plankton; higher nutrient uptake can translate to higher biomass accumulation among plankton, which then can produce higher amounts of POC export. As more POC is exported from the surface layer and sinks down to deeper layers, more respiration of POC occurs—thus leading to lower oxygenation of the overall ocean.

2.4.2 Grazing release from absence of large zooplankton can drive high carbon export

Larger size is often thought to correlate with larger carbon export; our model reveals an important exception to this rule. When phytoplankton of a community are larger than the zooplankton, the largest phytoplankton become free from grazing pressure, and they experience large blooms in biomass (see Supplementary Figure 2.2), which then drive extremely high rates of carbon export. This is a sheer biomass effect, which dominates over whatever increases in carbon export that may be contributed by adding larger size classes of zooplankton to a plankton community.

A plankton community experiencing blooms can be thought of as a community in a “perturbed” state (Falkowski et al. 2003). In our modern oceans, algal populations experience bloom and bust cycles; high rates of growth over mortality are eventually followed by high rates of mortality over growth, and this cycle repeats. Modern bloom events are indeed associated with high amounts of net carbon export to the ocean interior, particularly driven by diatoms (Falkowski et al. 2003; Falkowski et al. 1998). Another analog may be found in Precambrian oceans, before zooplankton were large enough to exert proper grazing control over phytoplankton (e.g., see Butterfield 1997 on microzooplankton-induced trophic cascades at the

Proterozoic-Phanerozoic transition; Figure 2.1).

2.4.3 Implications for export productivity through time and the mediating influence of tectonics

In Figure 2.4, we apply estimates of the range of possible maximum plankton sizes through time (Figure 2.1a) to our plots of plankton community carbon export from our model worlds (Figure 2.3, leftmost column) in order to draw implications from our model results for the overall arc of export productivity throughout the history of life. Simply taking one world into account (either the block world, left; the equator world, middle; or the polar world, right) we can hypothesize that export productivity is low in the Archaean (blue box) due to minimal sizes of life, drastically increases in the early and mid-Proterozoic (green box) as phytoplankton evolve larger sizes but face no grazing control from larger heterotrophic metazoans, slightly decreases in the late Proterozoic as larger metazoan heterotrophs evolve, and finally stabilizes throughout the Phanerozoic as plankton size classes stay relatively constant (Figure 2.4).

This contrasts with other views on transitions in export productivity through time in two ways. First, export productivity is generally assumed to have increased unidirectionally through time with the evolution of larger body sizes. However our model results point to the key importance of trophic *interactions* among differently sized things in driving carbon export, that modulate effects resulting from *individual* changes in body size. In particular, when size increases in zooplankton lag behind those in phytoplankton, the potential for grazing release, and thus significant blooms in phytoplankton biomass, result. Indeed, a reduction in carbon export at the Proterozoic-Phanerozoic transition, due to the evolution of larger zooplankton grazers and subsequent cascading trophic effects, has been proposed by Butterfield (1997).

Second, the relevance of plankton innovations in the Mesozoic to wider ecosystem and

biogeochemical changes throughout that time is widely discussed (e.g., Knoll & Follows 2016; Ward & Follows 2016). However, such shifts within the Phanerozoic are not indicated by our model results. It is possible that such shifts throughout the Phanerozoic are relatively too small in magnitude, compared to more dramatic changes spanning Earth history (e.g., the advent of cyanobacteria around the early Proterozoic or the evolution of metazoans around the late Proterozoic Cambrian), to be captured by our modeling framework. Also, importantly, our model does not parameterize for the specific plankton functions that have been proposed to drive Mesozoic transitions, including mixotrophy, silicification and calcification of plankton, and the more efficient and larger aggregation of organic matter in fecal pellets.

Figure 2.4 provides an excellent illustration for the potential effects of tectonic change in mediating size-based transitions in carbon export. To imagine export productivity throughout time, we cannot constrain ourselves to just the patterns of one model world. Rather, continental configuration has changed through time, and we might imagine jumping from one model world to another as geologic time progresses. Thus the hypothesis described above, taking only one world into account (low-to-high-to-slightly less high carbon export from the Archaean to the Phanerozoic), does not represent a hard and fast rule. Shifts in tectonic settings can decrease—or increase—the magnitude of export productivity changes from one time period to the next, or even, in the most extreme scenarios, alter the directionality of such changes.

2.5 Conclusion

Though our model worlds are highly idealized, they reveal crucial pivot points wherein the evolution of a plankton community's size structure can affect significant changes in carbon export and the strength of the biological pump, through mechanisms such as overall plankton

size increase as well as phytoplankton biomass accumulation. Such changes showcase the ability of biological and ecological interactions in the surface ocean to affect large-scale global processes such as the carbon cycle and have implications for the overall arc of export productivity, as well as perhaps primary productivity, throughout time.

2.6 Figures

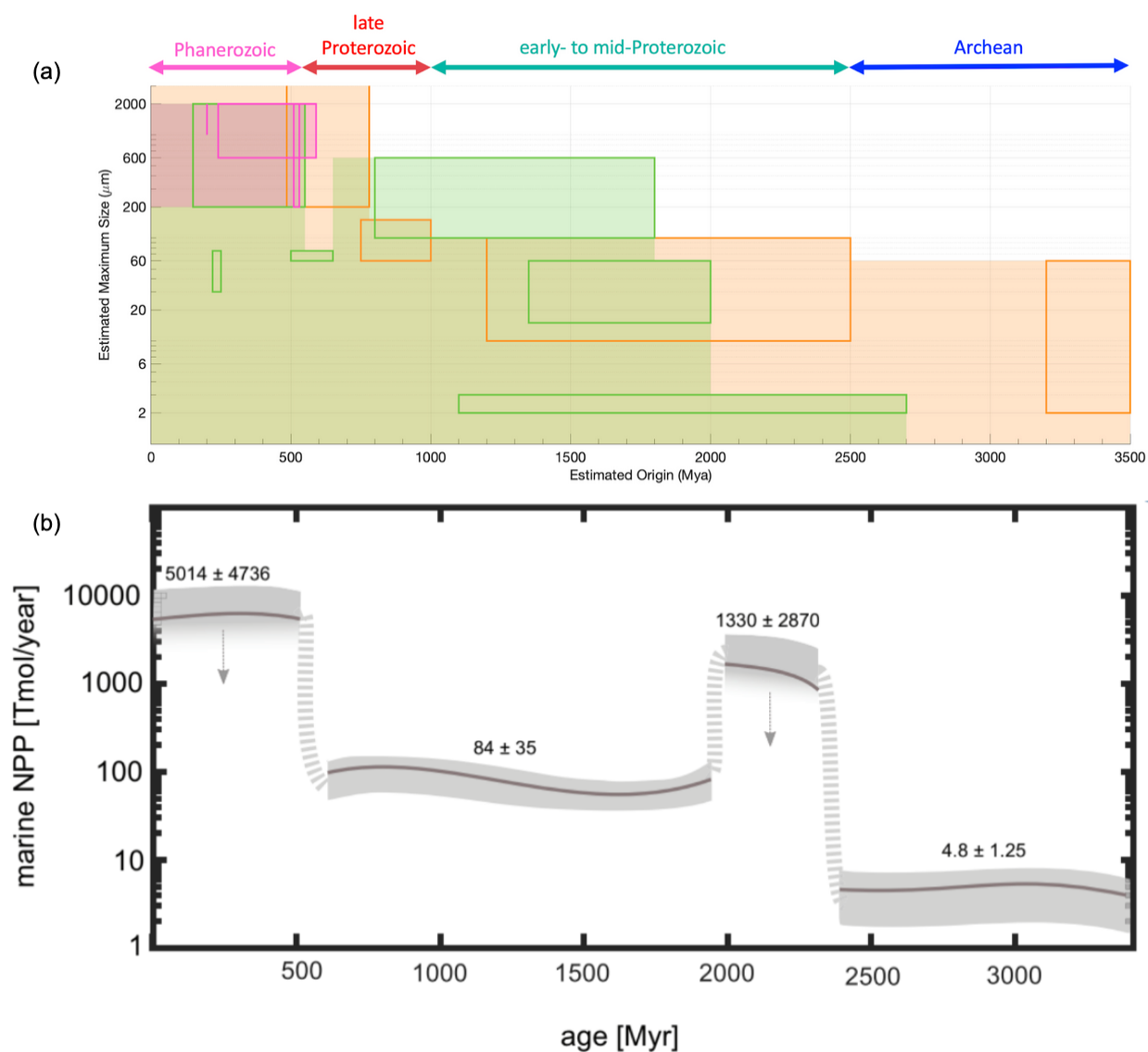


Figure 2.1: Possible correlation between (a) innovations in maximum plankton size and (b) marine net primary productivity through time. Please see Section S2.1 of Appendix 2 for additional short description. Green indicates “phytoplankton”; orange indicates “zooplankton”; and pink indicates mixotrophic strategies (see Section 2.2.3 for a note on terminology). Plankton size estimates were compiled from multiple sources; see Section S2.2 of Appendix 2 and Supplementary Table 2.1 for detailed methods and references. See Supplementary Figure 2.1 for detailed labels of different organismal groups corresponding to each box. Primary productivity estimates copied directly from Planavsky et al. (2022). See additional note on productivity estimates in Section S2.3 of Appendix 2. Color coding and labeling of time periods appears at the very top; this color coding scheme is applied to plots of plankton community carbon export in Figure 2.4.

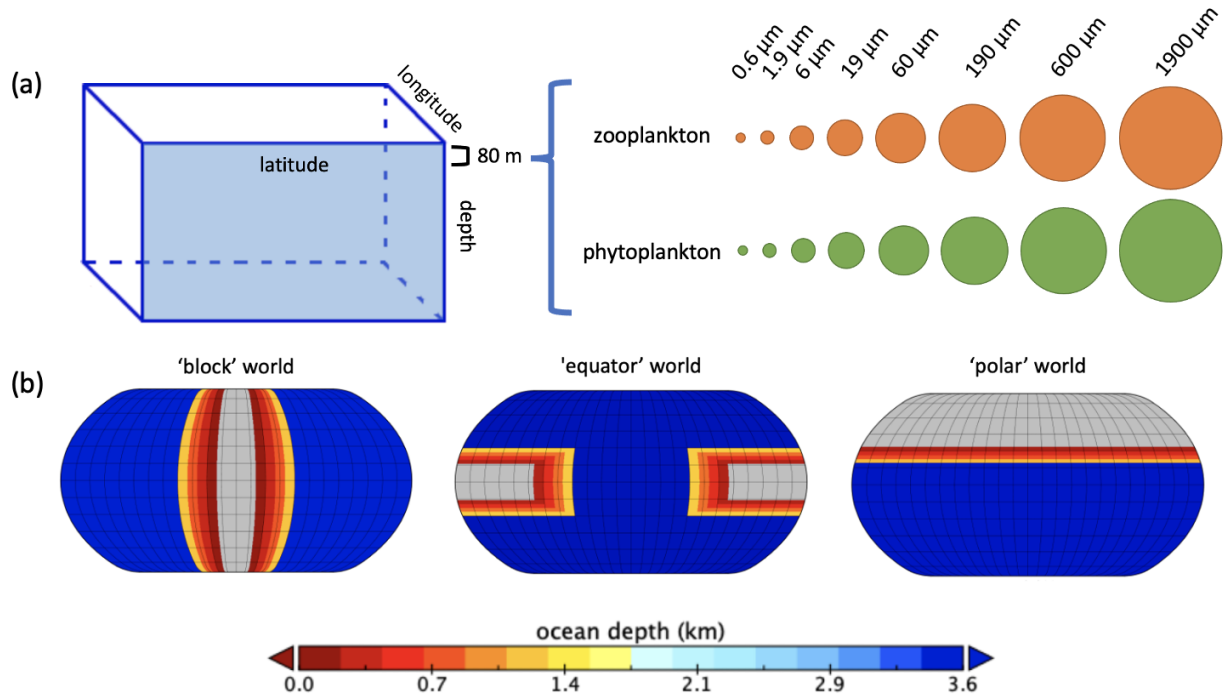


Figure 2.2: Simplified schematic of EcoGENIE plankton parameterization within the broader model cGENIE and idealized model worlds. (a) shows the parameterization of various plankton populations, defined by functional type and size, within the surface layer of the model ocean. Internal trophic interactions, nutrient uptake, and POM/DOM output from the plankton community exist but are not shown here; please see Ward et al. (2018) and Wilson et al. (2018) for more detailed schematics of the EcoGENIE model. (b) shows the continental configuration of our three idealized model worlds, explained in depth in Section 2.1 of this paper.

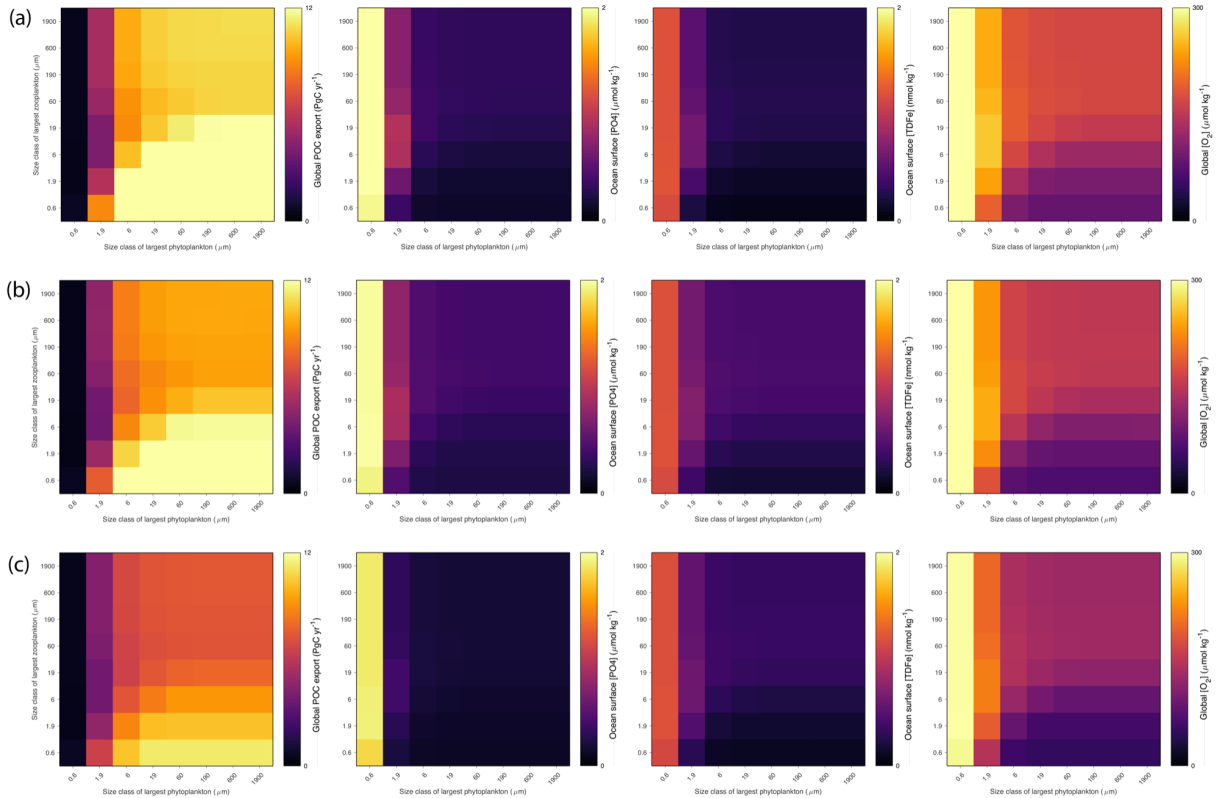


Figure 2.3: Global ocean mean particulate organic matter (POC) export (Pg C/year), surface ocean mean PO_4 concentration ($\mu\text{mol/kg}$), surface ocean mean Fe concentration (nmol/kg), and global ocean mean O_2 concentration ($\mu\text{mol/kg}$) for all 64 plankton community configurations in the (a) ‘block’ world, (b) ‘equator’ world, and (c) ‘polar’ world. Each individual grid cell represents a result from a particular model simulation, with the x-coordinate denoting the size class of the largest phytoplankton (μm) and the y-coordinate denoting the size class of the largest zooplankton (μm) for the simulation. Each simulated plankton community includes the largest phytoplankton population (as indicated on the x-axis) and all phytoplankton populations smaller than it, as well as the largest zooplankton population (as indicated on the y-axis) and all zooplankton populations smaller than it. As an example, the bottom right grid cell in each plot represents a plankton community with all 8 possible phytoplankton size classes and the 1 smallest zooplankton size class.

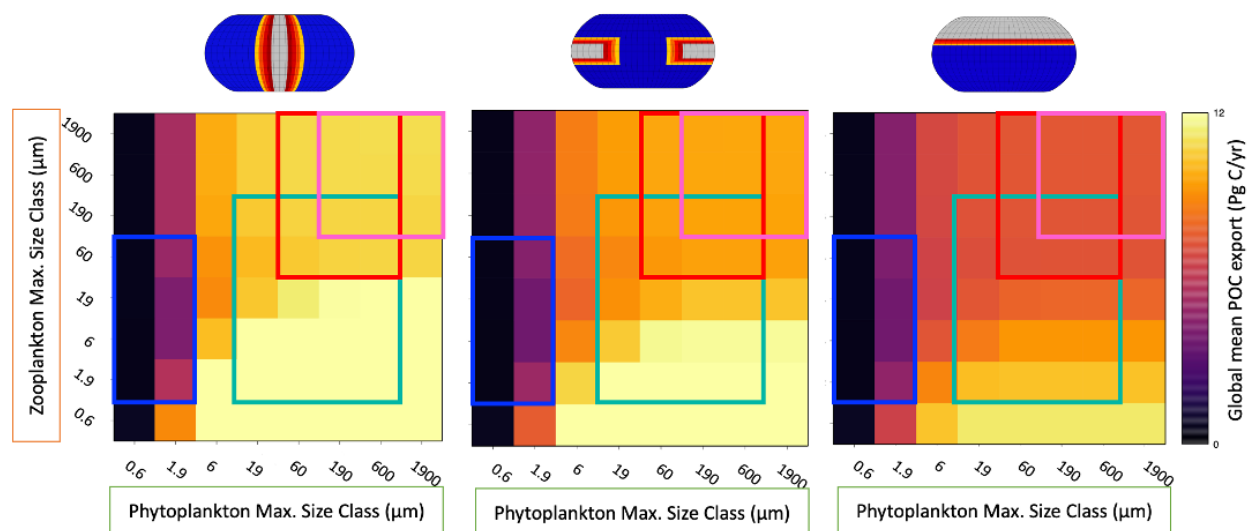


Figure 2.4: Mapping plankton size transitions through time (Figure 2.1a) onto modeled patterns in carbon export (Figure 2.3, leftmost column) for the (a) ‘block’ world, (b) ‘equator’ world, and (c) ‘polar’ world. As indicated by the color coding of time periods at the very top of Figure 2.1, blue represents a range of possible maximum plankton sizes for the Archean, green represents a range of possible maximum plankton sizes for the early to mid-Proterozoic, red represents a range of possible maximum plankton sizes for the late Proterozoic, and pink represents a range of possible maximum plankton sizes for the Phanerozoic.

Appendix 1

S1.1 Additional model information and references

The mid-layer and base of layer depths of each of the 16 logarithmically-scaled depth layer can be found at <https://github.com/derpycode/muffindoc/blob/master/muffin.pdf>, Figure 3.2 of Chapter 3. In the same document (Section 18.4 and 19.3.3), vertical/horizontal mixing is recommended for extreme continental configurations that are highly idealized.

S1.2 Diagnostic properties of model worlds at default environmental conditions

Here we discuss baseline conditions found in our three idealized worlds—block world, equator world, and polar world—at default environmental boundary conditions of 1x $p\text{CO}_2$, 1x $p\text{O}_2$, and 1x sinking rate (these parameters are described in Section 1.2.2 of the main text). We often reference details from the ‘modern’ world, which refers not to the real-life ocean but the model representation of it in cGENIE, after Crichton et al. (2020).

S1.2.1 Surface currents

The block world most closely resembles our modern ocean in terms of surface ocean circulation, with clear subtropical and subpolar gyres (Figure 1.1c) and surface currents extending a few hundred meters in depth (~400 m, Figure 1.1d). In contrast, the equator and polar worlds feature distinct high-speed circumglobal currents (two in the equator world at ~60°N and ~60°S and one in the polar world at ~60°S) and surface currents that extend markedly deeper (~1200 and ~800 m deep in the equator and polar worlds, respectively). The vertical extent of surface currents in the block world is comparable to the depth of most surface currents

in the modern world (~ 400 m), while surface currents in the equator and polar worlds show more similarity to modern surface currents in the Southern Ocean where they can reach ~ 800 m or even lower. Surface currents may extend more deeply in the idealized worlds due to more aggressive mixing caused by a combination of a simplified applied wind field and vertical/horizontal, rather than isopycnal/diapycnal, mixing.

The two idealized worlds with circumglobal currents have higher maximum surface current speeds closer to that of the modern world (equator - 0.081 m/s, polar - 0.080 m/s, modern - 0.086 m/s) than the block world, which features no circumglobal current (block - 0.070 m/s). The equator and polar worlds also have higher mean surface current speeds (equator - 0.027 m/s; polar - 0.031 m/s) than the block world, though ultimately all are roughly comparable to similarly gridded data in the modern (block - 0.024 m/s; modern - 0.025 m/s).

SI.2.2 Deep ocean flow

Vertical cross-sections of global streamfunction in the model oceans show varying patterns of deep ocean flow for all worlds (Figure 1.1d). In the block world, water subducts at both poles and upwells near the equator, forming two distinct partitions of water that flow in opposite directions beneath the surface currents. The position of the continent in the block world ensures that northward and southward flows of deep water are relatively uninterrupted. In the equator world, deep ocean flow is complicated by the presence of a continent between $\sim 30^\circ\text{N}$ and $\sim 30^\circ\text{S}$, with an open equatorial gateway that spans $\sim 60^\circ\text{W}$ to $\sim 60^\circ\text{E}$. Perhaps due to the continental configuration, surface currents at $\sim 45^\circ\text{N}$ as well as $\sim 45^\circ\text{S}$ extend more deeply as they hit the continental shelf. The strong mixing that results from such currents may disrupt deep ocean flows. In the equator world, water subducts in the south pole and upwells at the equator,

but the flow is much weaker and less direct than that found in the block world. The northern hemisphere ocean displays strong subduction at the north pole (more intense than that found at the south pole) and similarly weak upwelling at the equator. Finally, deep ocean flow in the polar world is limited by the placement of a continent covering a large section of the northern hemisphere, extending from the north pole down to $\sim 30^\circ\text{N}$ or $\sim 15^\circ\text{N}$ depending on the depth at which subsurface waters are interacting with the continental shelf. In the polar world there is one prominent movement of water, subducting at the south pole and upwelling at the equator.

SI.2.3 Temperature and salinity

Mean global ocean temperatures for the block, equator, and polar worlds are within 2°C of the mean global ocean temperature for the modern world (block - 1.9°C ; polar - 2.9°C ; equator - 4.1°C ; modern - 3.6°C). Latitudinal temperature gradients in the three idealized worlds are comparable to those found in the modern, with slightly lower average temperatures at both the poles and the equator. Temperatures range from -1.7°C at the equator to 25.2°C at the poles (averaged longitudinally) in the block world, -1.9°C to 25.8°C in the equator world, -1.9°C to 26.3°C in the polar world, and -1.5°C to 27.2°C in the modern world. Overall, the block world experiences the coldest temperatures and narrowest temperature range of all the idealized worlds, while the equator world experiences the warmest temperatures and widest temperature range. In all idealized worlds, the ocean is characterized by warmer surface waters centered at the equator and near-freezing temperatures everywhere else (Supplementary Figure 1.2a). The vertical extent of these warmer surface waters differs among all three worlds, much like the vertical extent of the surface currents. In the block world, temperatures above $\sim 10^\circ\text{C}$ occur as deep as ~ 500 m, while the equator and polar worlds feature elevated temperatures as deep as ~ 800 m.

The block, equator, and polar worlds experience a narrower range of salinities than the modern world. While maximum salinities are comparable (block - 35.3 PSU; equator - 35.6 PSU; polar - 35.4 PSU; modern - 35.5 PSU), the idealized worlds have higher minimum salinities than the modern (block - 34.5 PSU; equator - 34.4 PSU; polar - 34.3 PSU; modern - 32.3 PSU). In all idealized worlds, highest salinities are found in low latitudes near the equator and lowest salinities are found in high latitudes near the poles (Supplementary Figure 1.2). In the block world, salinity gradients are roughly symmetrical between the northern and southern hemispheres. Pools of saltier water exist between 60°N and 60°S of the equator, and they extend down to ~800 m in the ocean. Meanwhile, pools of less salty water exist near both poles and extend down to ~400 m in the ocean. These patterns are likely due to relatively even subduction of polar water and upwelling near the equator in both hemispheres. In contrast, the ‘equator’ and ‘polar’ worlds show greater differences in the distribution of salinity between hemispheres. In the equator world, fresher water at the poles extends more deeply and more southward in the northern hemisphere, while saltier water near the equator extends more deeply and more southward in the southern hemisphere. This disparity may reflect the equator world’s asymmetrical deep ocean flow patterns (e.g., particularly strong subduction in the north pole). A similar pattern is found in the polar world, where saltier waters are deeper and more extensive in the southern hemisphere than the north. In contrast, however, fresh waters are restricted in the northern hemisphere to just above the top two steps of the continental shelf.

SI.2.4 Nutrients and productivity

PO₄ concentrations in the block, equator, and polar worlds are noticeably higher and more wide-ranging than in the modern world (Supplementary Figure 1.2). In the block world, nutrients

are most concentrated at the equator near the surface, reaching a maximum of 3.1 $\mu\text{mol/kg}$ (averaged latitudinally). In the equator world, nutrients are most concentrated in the subpolar region of the northern hemisphere, close to the seafloor, reaching a maximum of 3.0 $\mu\text{mol/kg}$. There are also substantial nutrients at the equator near the surface at concentrations of ~ 2.7 $\mu\text{mol/kg}$. In the polar world, nutrients reach maximum concentrations of 3.4 $\mu\text{mol/kg}$. They are concentrated at the equator near the surface, similar to the block world, but also extend northward in subsurface waters and hit the continental shelf. The modern world does not feature comparably high nutrient concentrations so close to the ocean surface. Similarly, productivity, in the form of POC flux density, appears noticeably higher in the block, equator, and polar worlds than in the modern world (Supplementary Figure 1.2). This may be due to stronger equatorial and continental upwelling in the three idealized worlds than in the modern. Deeper mixing in the idealized worlds may entrain nutrients and POC in the surface ocean rather than allowing them to sink. Excess PO_4 may also result from Fe limitation as productivity in the idealized worlds is both PO_4 - and Fe-limited.

SI.2.5 Ocean oxygen and euxinia

The block, equator, and polar worlds experience much lower minimum O_2 concentrations than the modern world (block - 13.0 $\mu\text{mol/kg}$; equator - 2.1 $\mu\text{mol/kg}$; polar 0.0 $\mu\text{mol/kg}$; modern - 85.0 $\mu\text{mol/kg}$), as well as higher maximum H_2S concentrations (block - 15.4 $\mu\text{mol/kg}$; equator - 43.5 $\mu\text{mol/kg}$; polar - 78.2 $\mu\text{mol/kg}$; modern - 2.1 $\mu\text{mol/kg}$) (Supplementary Figure 1.2). The three idealized worlds also feature well-developed and extensive oxygen minimum zones, centered below and extending beyond the equatorial upwelling zone (Supplementary Figure 1.2). The shape and depth of the oxygen minimum zones are reflective of other patterns in nutrient

distribution and ocean circulation. Using a cutoff of $< \sim 100 \mu\text{mol/kg}$ (O_2 values are averaged across longitudes), the OMZ extends from $\sim 20^\circ\text{S}$ to $\sim 20^\circ\text{N}$ and is ~ 1100 m deep in the block world. The OMZ extends from $\sim 20^\circ\text{S}$ to $\sim 20^\circ\text{N}$ and is ~ 1300 m deep in the equator world, and extends from $\sim 15^\circ\text{S}$ and $\sim 30^\circ\text{N}$ and is ~ 1300 m deep in the polar world. Meanwhile, the OMZ in the modern world only extends from $\sim 10^\circ\text{S}$ to $\sim 10^\circ\text{S}$ and is ~ 850 m deep. As in the modern world, OMZs are concentrated along the continental shelf of each of the three idealized worlds; however, the three idealized worlds differ in which parts of the shelf are impacted by the OMZ (Supplementary Figure 1.3). For example, in the equator world, water with $< 15 \mu\text{mol/kg}$ O_2 is found on the top three steps of the continental shelf, while in the polar world, such low-oxygen water only directly interacts with the third step of the continental shelf. Euxinic zones are found at the cores of these OMZs where oxygen is depleted. Overall, the three idealized worlds are characterized by much greater anoxic and euxinic ocean conditions than the modern world, with particularly strong OMZs and euxinic zones found in the equator and polar worlds.

SI.2.6 Sea ice

Each of the idealized worlds feature roughly 5 to 10% surface sea ice cover (Supplementary Figure 1.4a). The most extensive sea ice cover is found in the equator world (11.1% of surface grid cells contain some amount of sea ice), followed by the block world (8.0%), and polar world (5.6%). The thickest sea ice is found in the block world, reaching up to 5 m thick, in comparison to maximums of ~ 4 m in other worlds (Supplementary Figure 1.4b). In all idealized model worlds, except the equator world, sea ice cover reduces to 0% at $4\times \text{CO}_2$ (1112 ppm). Sea ice cover is 0% for all idealized model worlds at $8\times \text{CO}_2$ (2224 ppm). Particulate organic carbon flux (POC) is negligible throughout the water column under sea ice,

due to the model assumption of no productivity under the ice.

For ease of discussion of these 360 possible model configurations, we choose one continental configuration and one combination of environmental factors as our default, or base, simulations to examine in detail before introducing other simulations for comparison and contrast. We treat the block world as our default continental configuration because its continental shelf spans the full range of latitudes and features the widest diversity of potential habitat.

S1.3. Additional description of isolated and combined effects of continental configuration, atmospheric $p\text{CO}_2$, atmospheric $p\text{O}_2$, and sinking rate on benthic shelf oxygenation

S1.3.1 Isolated effects of continental configuration on benthic shelf oxygenation

In default conditions, some parts of the benthic shelf experience low- O_2 conditions (0 to 15 $\mu\text{mol O}_2/\text{kg}$) in all three idealized worlds (Supplementary Figure 1.6a, e, i; identical to Supplementary Figure 1.7a, g, m and Supplementary Figure 1.8a, f, k). In the block world, low- O_2 conditions occur in relatively low latitudes on the shallowest shelf steps on the eastern and western sides of the continent (Supplementary Figure 1.6a), with a general tendency towards more latitudinally extensive low- O_2 conditions with increasing shelf depth. The block world also displays notable differences in the depth and latitudinal extent of low- O_2 conditions along eastern and western continental bounds: in the west, low O_2 conditions extend deeper, reaching the fourth step, but are latitudinally more restricted than in the east. Unlike the block world, the equator world does not feature any low- O_2 conditions on the deepest step of the continental shelf under default conditions (Supplementary Figure 1.6e). Low- O_2 conditions in the equator world are also distributed differently along the short (i.e., eastern and western) and long (i.e., northern and southern) coasts of the continent. In the polar world, the first, second, and fourth steps of the

continental shelf are relatively well-oxygenated, experiencing no low-O₂ conditions (Supplementary Figure 1.6i), though the entire length of the third step is characterized by low O₂.

S1.3.2 Isolated effects of atmospheric pCO₂ on benthic shelf oxygenation

Different steps of the continental shelf respond differently to changes in atmospheric pCO₂ in all model worlds. In the block world, doubling pCO₂ tends to expand the extent of low-O₂ conditions on the shallowest two steps, while limiting (and, in some cases, eliminating) low-O₂ conditions on the deepest two steps of the shelf (Supplementary Figure 1.6b-d). Variations along the eastern and western boundaries of the continent remain. Similar responses to CO₂ doubling occur in the equator world (Supplementary Figure 1.6f-h) and the polar world (Supplementary Figure 1.6j-l), with the equator world experiencing additional slight variations along all boundaries of the continent as well.

S1.3.3 Isolated effects of atmospheric pO₂ on benthic shelf oxygenation

In all worlds, incremental decreases in atmospheric pO₂ decidedly increase low-O₂ conditions on the shelf (Supplementary Figure 1.7), though the exact steps affected and the levels of atmospheric pO₂ responsible for the greatest declines in shelf oxygenation vary (also indicated by Supplementary Figure 1.3b). In the block world, all steps of the continental shelf experience low-O₂ conditions once atmospheric pO₂ is decreased to 50% PAL (Supplementary Figure 1.7c). In the equator world, low-O₂ conditions begin to affect the entire continental shelf at 0.4x O₂, or 40% PAL (Supplementary Figure 1.7l). In the polar world, the shallowest continental shelf step is relatively unresponsive to decreases in atmospheric pO₂ and does not experience low-O₂ conditions even at 0.2x O₂ (Supplementary Figure 1.7r). In contrast, the bottom two steps of the

continental shelf in the polar world have low-O₂ conditions at 0.75x O₂ (Supplementary Figure 1.7n), and the lowest three steps at 0.5x O₂ (Supplementary Figure 1.7o).

S1.3.4 Isolated effects of sinking rate on benthic shelf oxygenation

Generally, slower sinking rates serve to oxygenate the continental shelf in each idealized world and decrease the amount of benthic shelf with low-O₂ conditions (Supplementary Figure 1.8). However, there are exceptions to this trend, dependent on the specific continental configuration and the steps of the continental shelf being considered. Overall, the block world follows the trend, with greater oxygenation of all steps of the benthic shelf resulting from slower sinking rates. The equator world, however, only shows reductions in low-O₂ regions on the deepest three steps of its continental shelf as sinking rate slows. The extent of low-O₂ on the equator world's shallowest shelf step increases with lower sinking rates (Supplementary Figure 1.8i-j). Similarly, the shallowest two steps of the polar world become slightly less oxygenated as sinking rate slows, while its deepest two steps become more oxygenated.

S1.3.5 Combined effects of tectonic and environmental factors on fraction of anoxic benthic shelf area

Here we consider results from all 360 model experiments (Supplementary Figure 1.9, showing same data presented in Figure 1.4 in a different format). At first glance we can see that continental configuration places broad controls on how a world is affected by changing atmospheric pO_2 and sinking rate. In the block world, the range of anoxic benthic area percentages ranges from ~10 to ~70%. In the equator world, the range is ~20 to ~100%. In the polar world, the range is ~10 to ~100%.

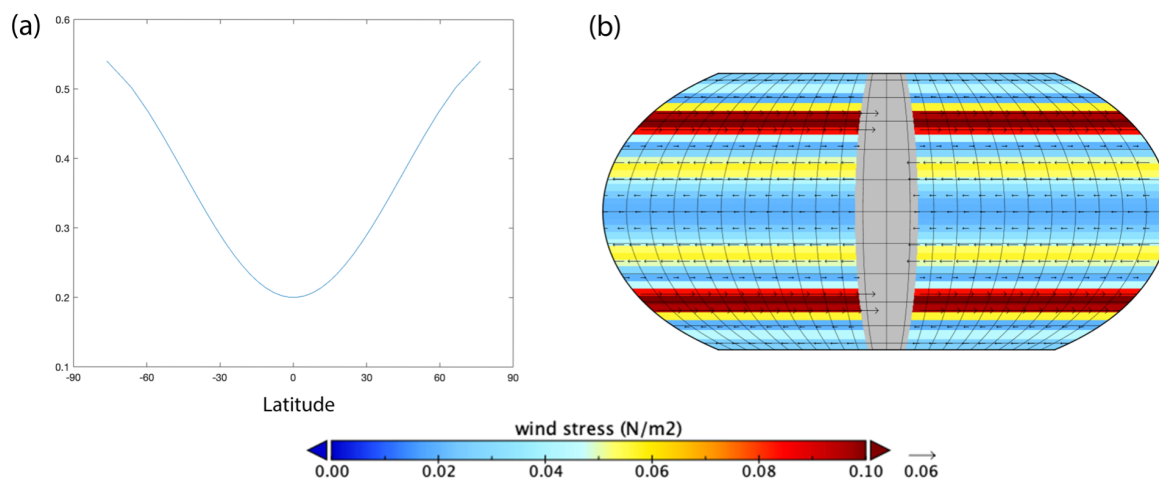
Next we can once again identify the importance of atmospheric pO_2 in maintaining potential oxic habitat availability even when other factors are changing. All worlds are most stably oxygenated at 1.0x pO_2 (100% PAL; benthic anoxia remains relatively limited (~0 to ~30% for the block world, ~20 to ~30% for the equator world, and ~0 to ~30% for the polar world) even as all other environmental factors (atmospheric pCO_2 and sinking rate) change.

Finally we can identify some important interacting effects among pO_2 and sinking rate in each world. In the block world, sinking rate influences the extent of anoxia on the benthic shelf along with pO_2 , although the range of these responses is still ultimately limited by pO_2 (e.g., percentages >70% can only be reached once pO_2 has decreased to a certain point) (Supplementary Figure 1.9a-d). In the equator world, sinking rate also interacts with pO_2 to influence benthic anoxia, but is dominated by pO_2 as the main benthic anoxic control at lower pO_2 conditions (as evidenced by the vertical contour lines, Supplementary Figure 1.9e-h). The same can be said for the polar world, which exhibits some responses to sinking rate at higher pO_2 conditions but not lower ones (Supplementary Figure 1.9i-l).

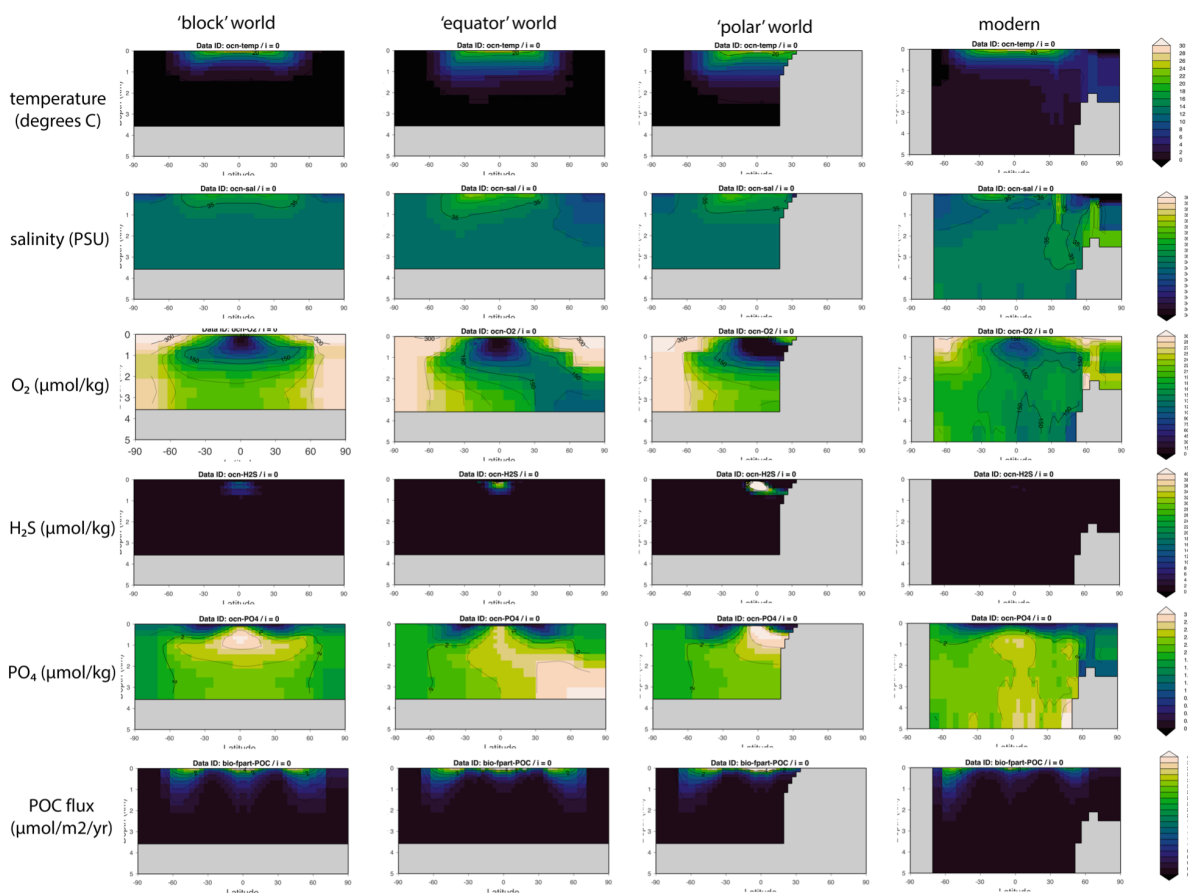
Supplementary Table 1.1

	Global ocean volume (km³)	Global ocean surface area (km²)	Global average ocean temperature (°C)	Global average ocean O₂(μmol/kg)	Global average ocean PO₄(μmol/kg)	Total POC export (Pg C/yr)
‘block’ world	1,285,507,000	453,248,300	1.9	197	2.2	14
‘equator’ world	1,286,760,000	446,953,200	2.9	187	2.2	15
‘polar’ world	1,250,487,000	396,592,300	4.1	184	2.1	16
modern	1,302,484,000	367,477,400	3.6	175	2.2	8

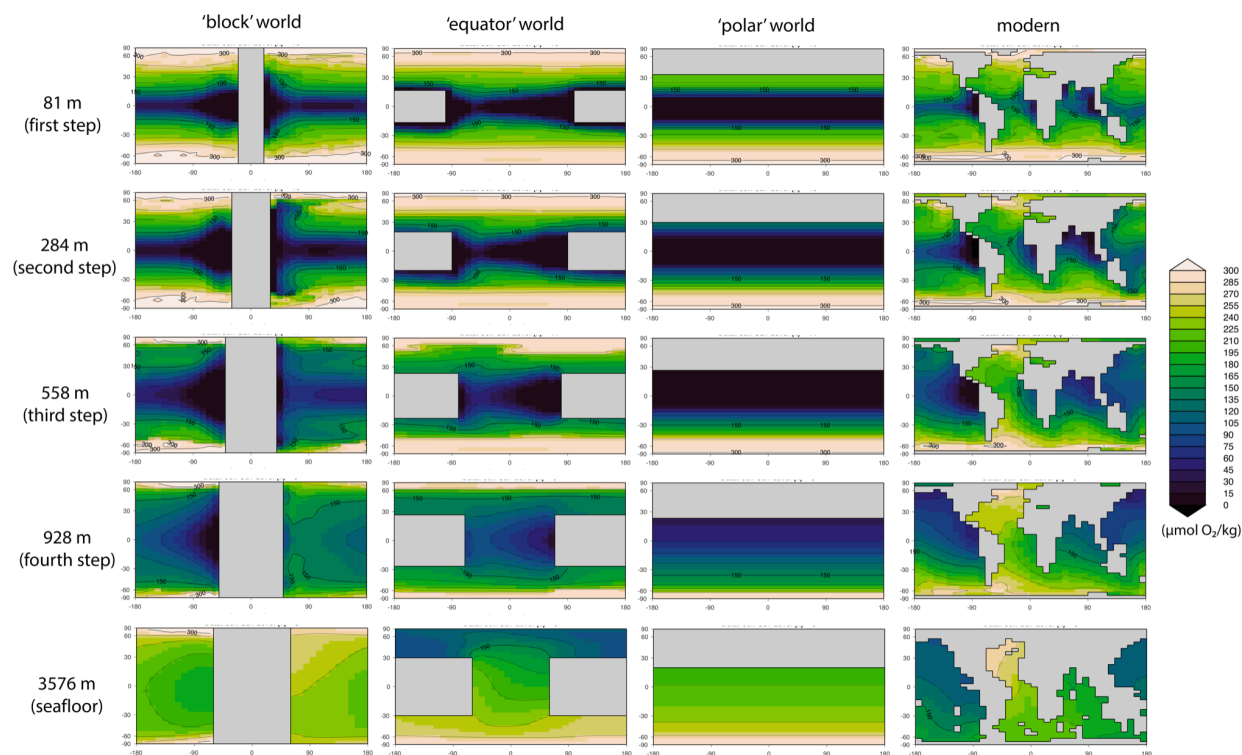
Supplementary Table 1.1: Global summary statistics for each idealized continental configuration at default environmental conditions (i.e., pre-industrial modern $p\text{CO}_2$, modern $p\text{O}_2$, and modern sinking rate), with modern world for comparison. Global ocean volume and global ocean surface area are listed to seven significant figures, global average ocean temperature and global average ocean PO_4 to two significant figures, and global average ocean O_2 and total POC export as whole numbers.

Supplementary Figures 1.1 to 1.9

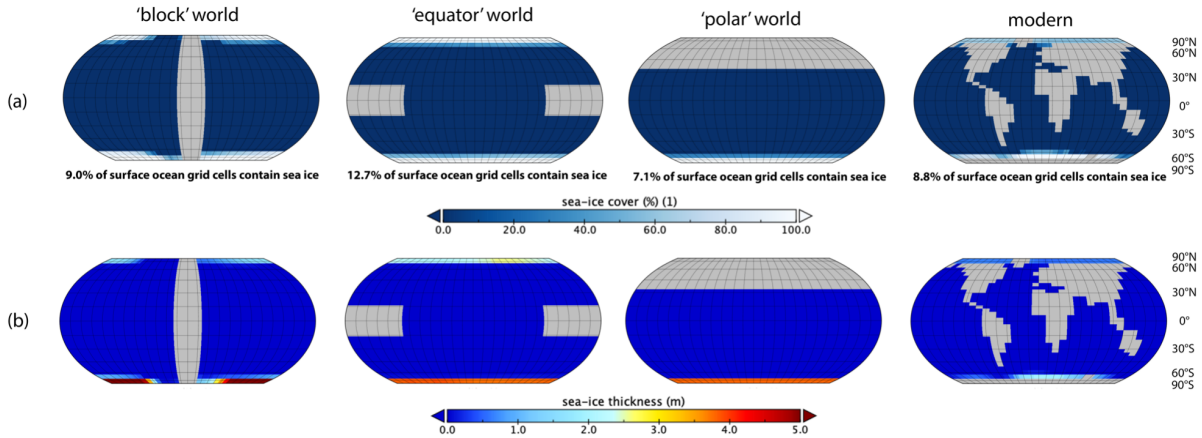
Supplementary Figure 1.1: Prescribed albedo profile and wind stress field for all idealized model worlds. (a) Latitude on the x-axis and albedo on the y-axis. (b) The intermediate zonal wind stress field as applied to a model world in the ‘block’ continental configuration with arrows indicating direction and colors indicating magnitude. Vertical gridlines mark longitude in increments of 15 E-W and horizontal gridlines mark latitude in increments of 15 N-S.



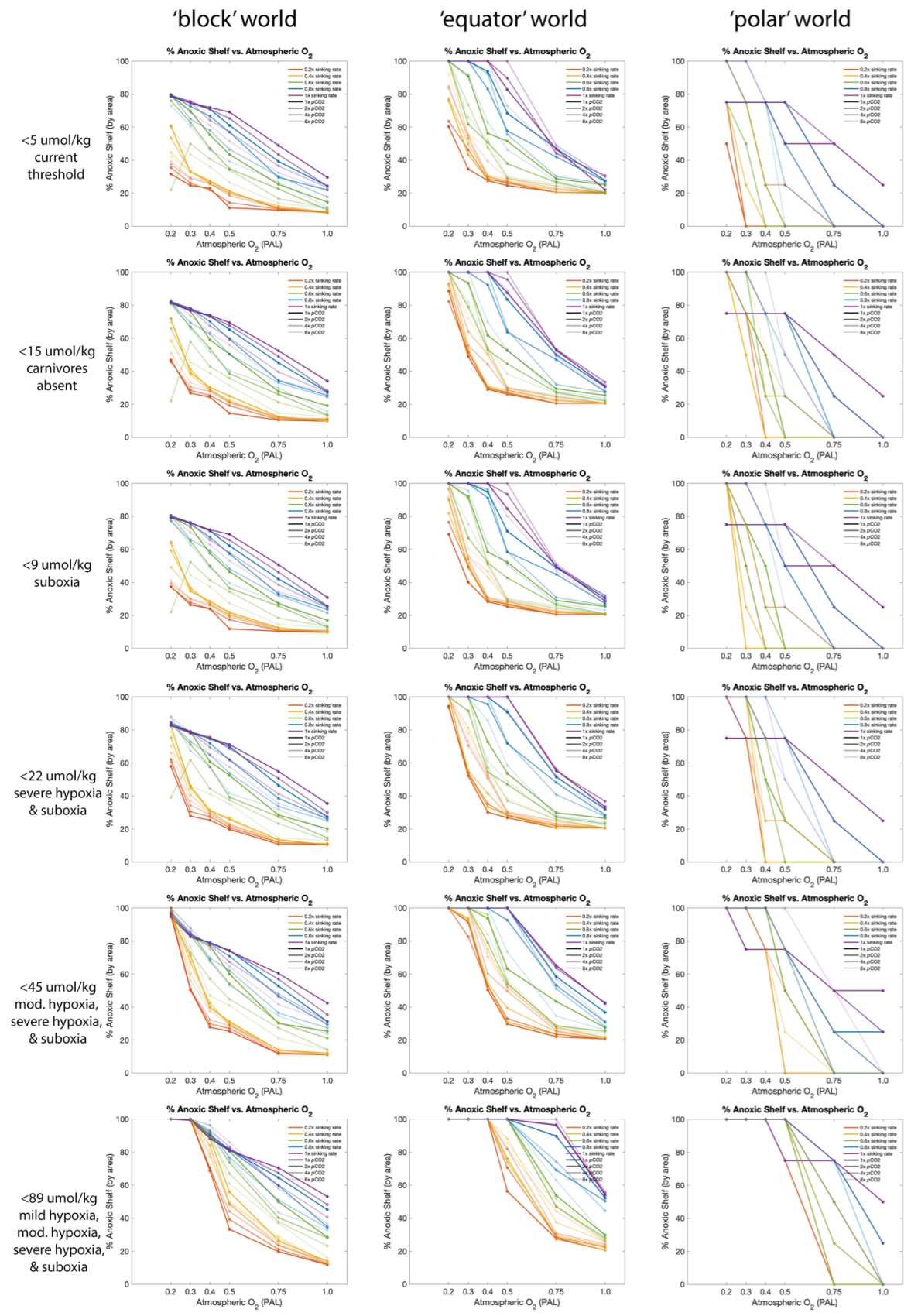
Supplementary Figure 1.2: Temperature, salinity, O₂, H₂S, PO₄, and POC flux for each idealized continental configuration at default environmental conditions, with modern world for comparison. Vertical slices (latitude on x-axis, depth on y-axis) of each world, with values averaged across all longitudes, are shown.



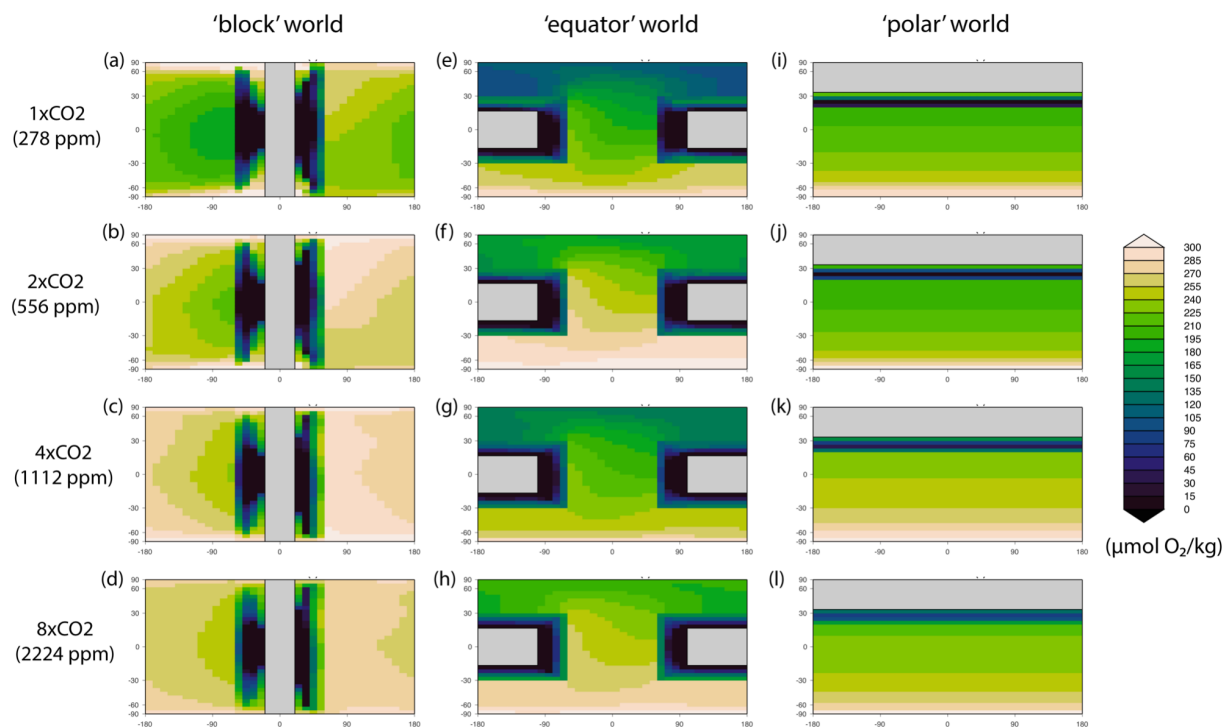
Supplementary Figure 1.3: Extent of OMZ relative to the four steps of the continental shelf and seafloor for each idealized continental configuration at default environmental conditions, with modern world for comparison. Dark colors (indigo to black) indicate areas of low marine oxygen. Horizontal slices (longitude on x-axis, latitude on y-axis) of each world, at the depths of each continental shelf step and the sea floor, are shown.



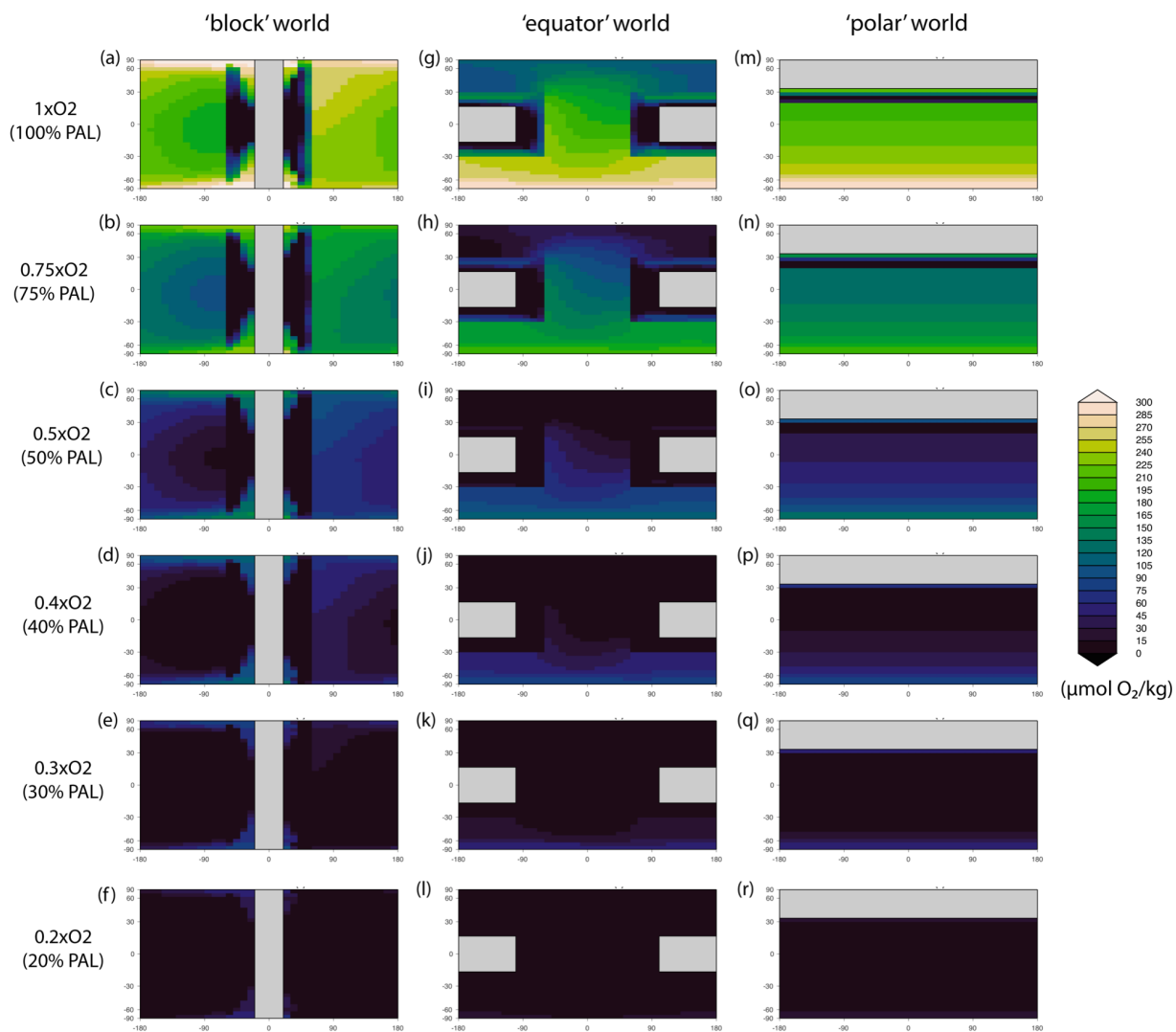
Supplementary Figure 1.4: Sea ice coverage and sea ice thickness for each idealized continental configuration at default environmental conditions, with modern world for comparison. Vertical gridlines mark longitude in increments of 15 E-W and horizontal gridlines mark latitude in increments of 15 N-S.



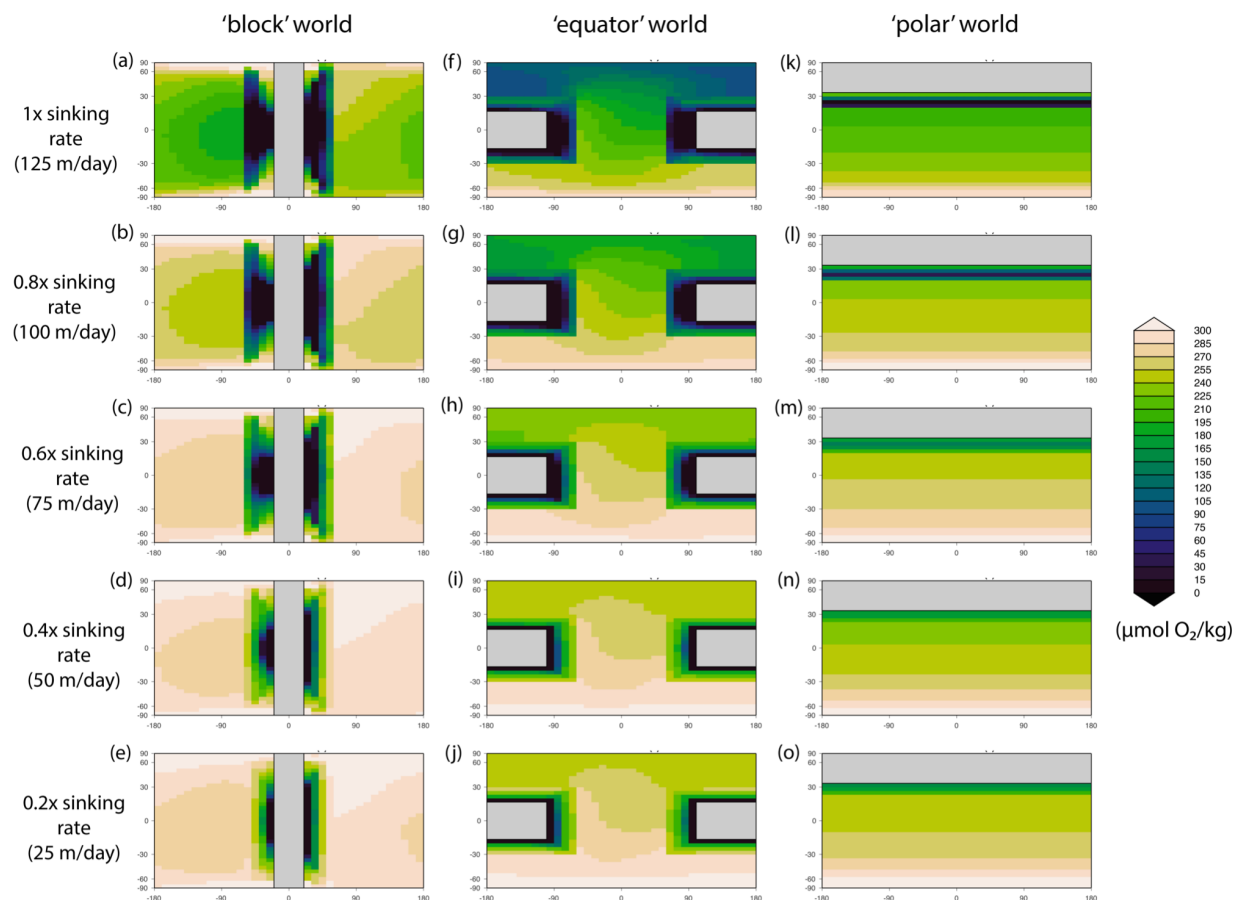
Supplementary Figure 1.5: Sensitivity of results (as expressed in Figure 1.4) to threshold for anoxic conditions. Alternative thresholds for anoxic conditions are taken from Sperling et al. (2013).



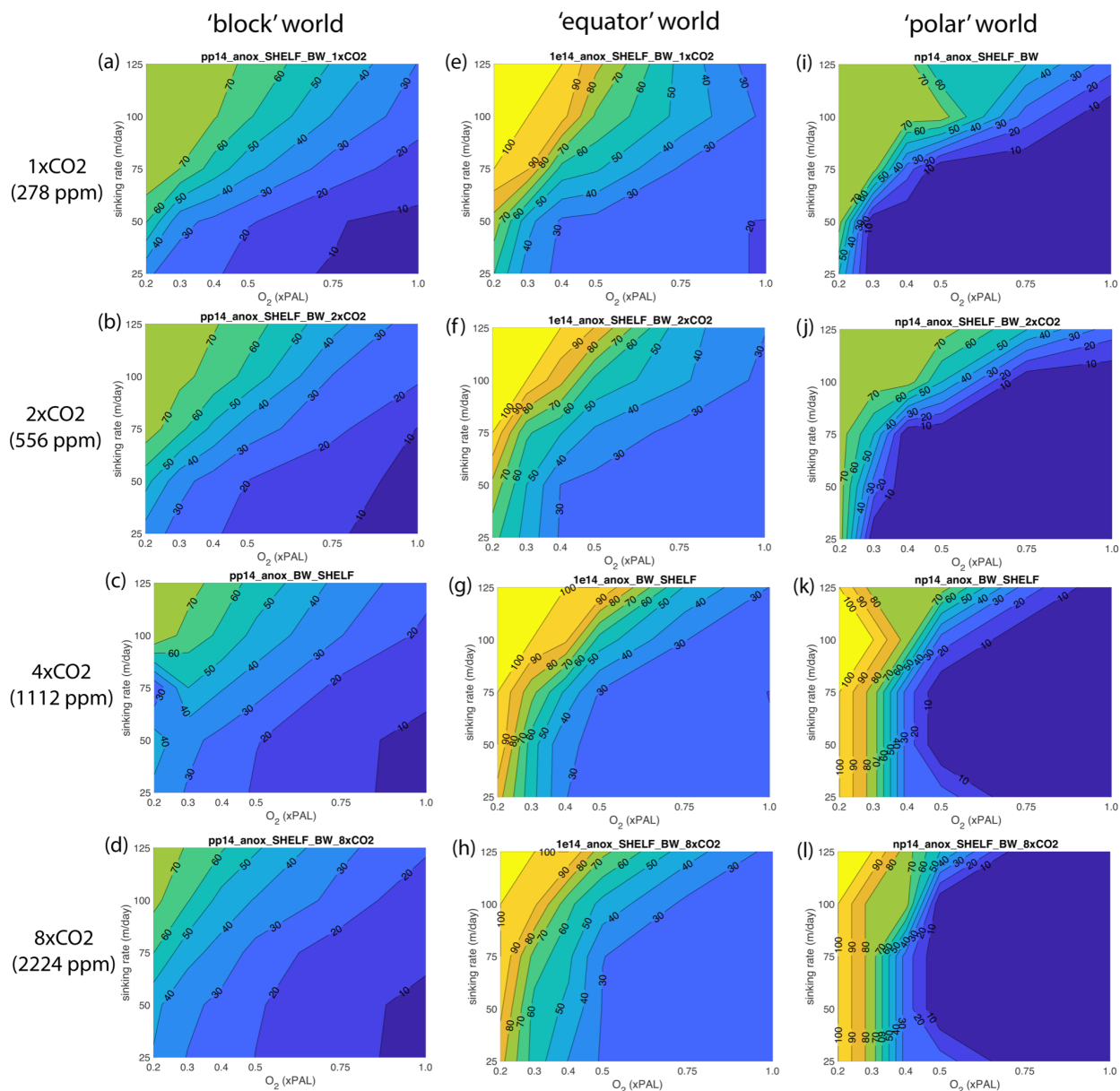
Supplementary Figure 1.6: The effect of CO₂ on O₂ concentrations on the benthic surface (i.e., four shelves and seafloor) of each idealized world, with default atmospheric pO_2 (1x, 100% PAL) and sinking rate (1x, 125 m/day). Dark colors (indigo to black) indicate areas of low marine oxygen on the benthic surface. Longitude-latitude is shown, with values labeled on each axis.



Supplementary Figure 1.7: The effect of atmospheric pO_2 on O_2 concentrations on the benthic surface (i.e., four shelves and seafloor) of each idealized world, with default atmospheric pCO_2 (1x, 278 ppm) and sinking rate (1x, 125 m/day). Dark colors (indigo to black) indicate areas of low marine oxygen on the benthic surface. Longitude-latitude is shown, with values labeled on each axis.



Supplementary Figure 1.8: The effect of sinking rate on O₂ concentrations on the benthic surface (i.e., four shelves and seafloor) of each idealized world, with default atmospheric $p\text{CO}_2$ (1x, 278 ppm) and atmospheric $p\text{O}_2$ (1x, 100% PAL). Dark colors (indigo to black) indicate areas of low marine oxygen on the benthic surface. Longitude-latitude is shown, with values labeled on each axis.



Supplementary Figure 1.9: Fraction of anoxic area on the benthic continental shelf for all tectonic and environmental configurations of each idealized world. Contour lines and their corresponding colors indicate the % anoxic shelf found at each combination of continental configuration, atmospheric $p\text{CO}_2$, atmospheric $p\text{O}_2$, and sinking rate. Sinking rate and $p\text{O}_2$ settings are indicated on the y-axis and x-axis, respectively, of each plot. Each row shows a different set of $p\text{CO}_2$ settings. Each column is labeled with the continental configuration. Anoxia is defined as oxygen concentrations below 5 $\mu\text{mol/kg}$.

Appendix 2

S2.1 Possible correlation between plankton size and productivity

Links between plankton evolution, innovations, and extinction and the broad arc of productivity through time is a focus of our future work. This section serves an additional note on the information presented in Figure 2.1.

The size of plankton has not been constant through Earth history (Figure 2.1a; see also Section S2.2 of Appendix 2 and Supplementary Figure 2.1), and changes in the maximum size of planktic organisms may correlate with broad trends in productivity through time, though estimates for productivity through time are relatively unconstrained (Figure 2.1b; see also Section 2.3 of Appendix 2). For example, low productivity in the Archaean is accompanied by minimal sizes in plankton. The Archaean featured small early prokaryotic planktic organisms, typically under 60 μm , and even smaller early cyanobacteria, typically under 3 μm . Relatively higher productivity in the Proterozoic is accompanied by a multitude of changes in the size of plankton. Early eukaryotic planktic organisms appear, and cyanobacteria experience a size increase of over one order of magnitude, to ~ 60 μm . The rise of acritarchs, commonly interpreted to be phytoplankton, in the mid- to late Proterozoic represent another step change in plankton sizes by an order of magnitude, reaching up to 600 μm . Finally, many innovations in plankton accompany an increase in productivity at the Proterozoic-Phanerozoic transition, including the rise of metazoans and “modern” plankton groups such as diatoms, dinoflagellates, and planktic foraminifera, which represent yet another increase in sizes, up to 2000 μm or more.

S2.2 Estimates of plankton size through time

S2.2.1 Scope and evidence

In their investigation of the origins, evolution, and diversification of zooplankton through time, Rigby & Milsom (2000) describe two important properties of plankton: a pelagic position and planktic habit. We follow similar guidelines in compiling hypotheses and evidence for the origin and maximum size of planktic organisms, as shown in Figure 2.1a and Supplementary Figure 2.1. Though distinguishing between pelagic and benthic existences for past life is highly ambiguous and uncertain, we do our best to prioritize hypotheses and evidence of the *pelagic* (or at the very least, non-benthic) origins and appearances of groups when possible.

We incorporate many lines of evidence, as may be evident in the large ranges of both pelagic origin/appearance and maximum size class for each group. These include fossil evidence, biomarker dates, phylogenetic reconstructions, and isotope evidence. Specific references—and lines of reasoning—for the content shown in Figure 2.1a and Supplementary Figure 2.1 are detailed in Supplementary Table 2.1.

Reviews of plankton and planktic ecosystems were particularly helpful, on the evolution of phytoplankton (Katz et al. 2007; Knoll et al. 2007), zooplankton (Rigby & Milsom 2000), and pelagic trophic structures (Lipps & Culver 2002) through time. Also helpful were reviews on early life (Knoll et al. 2016), specific investigations into pelagic cyanobacteria (Sánchez-Baracaldo 2015; Hurley et al. 2021), and eukaryote origins (Cohen & Kodner 2021; Knoll 2014).

S2.3 Estimates of productivity through time

S2.3.1 Productivity estimates through time

The arc of global primary productivity through time is a subject of great interest that is, at the same time, difficult to constrain. However, multiple investigations from the past few decades have contributed to our understanding of how production from the biosphere has changed throughout Earth history.

Overall there is relative consensus on major shifts in productivity—spanning one or multiple orders of magnitude—through time, and these are reflected in Figure 2.1b (Planavsky et al. 2022). Here we first present studies that concern specific time periods or events throughout history; we then compare these to overall estimates for productivity through time by Ward et al. (2018) and Planavsky et al. (2022). For the Archaean and parts of the Proterozoic prior to the Great Oxidation Event (GOE, ~2.4 to 2.0 Ga), productivity is estimated to be ~3 orders of magnitude lower than present; error allows for productivity as high as ~1 order of magnitude lower than present and almost ~4 orders of magnitude lower than present. Kharecha et al. (2005) and Canfield et al. (2005) incorporate estimates of phosphorus limitations and burial efficiency during the Archaean, and make calculations of productivity from anaerobic metabolisms, which are expected to have dominated, at the very least, from ~3.8 to 3.0 Ga in the early and mid-Archaean. The GOE consequently represents an abrupt increase in productivity, to within ~1 order of magnitude lower than present; this is supported by triple oxygen isotope evidence presented by Hodgskiss et al. (2019). A shift to lower productivity following the GOE, around ~1 to ~2 orders of magnitude lower than present, is also reflected in Hodgskiss et al. (2019) and Crockford et al. (2018) via triple oxygen isotope evidence. Such estimates of low productivity last into the Neoproterozoic (Wei et al. 2021). A possible source of (relatively minor, i.e.,

changes not spanning multiple orders of magnitude) productivity fluctuations in the Proterozoic may be the snowball Earth glaciations (e.g., Wei et al. 2021; Kunzmann et al. 2013). Finally, the Phanerozoic experiences productivity near modern levels, with relatively minor fluctuations (compared to the other, previously described productivity shifts through Earth history) that generally stay within ~1 order of magnitude of present levels (Wing 2013; Beerling 1999). Phanerozoic fluctuations in productivity that have been proposed are generally linked to perturbations in the biosphere or biogeochemical cycles; there is much literature surrounding possible productivity changes around the Permian-Triassic mass extinction (e.g., Wang et al. 2021; Grasby et al. 2016; Shen et al. 2014; Meyer et al. 2011), the Cretaceous-Paleogene mass extinction (e.g., Rosenberg et al. 2021; Hull & Norris 2011; Sepúlveda et al. 2009; Zachos et al. 1989), and the Paleocene-Eocene Thermal Maximum (e.g., Bridgestock et al. 2019; Winguth et al. 2012; Torfstein et al. 2010; Stroll et al. 2007; Gibbs et al. 2006). Other fluctuations may relate to animal radiations and widespread euxinia in the Cambrian (e.g., Dahl et al. 2019; Gill et al. 2011) as well as glacial-interglacial cycles (Bender et al. 1994; Paytan et al. 1996).

Ward et al. (2018) and Planavsky et al. (2022) provide estimates of primary productivity throughout the whole of Earth history using different methods. What is notable about these long-ranging estimates when comparing them to studies of specific time periods or featuring empirical data (e.g., isotopes) tied to a specific moment in time is that all of them agree to some extent. Agreement on the major step changes in productivity through time exists even with uncertainties and errors in empirical approaches (e.g., with triple oxygen isotopes, Liu et al. 2021).

S2.3.2 Export productivity and primary productivity

Productivity estimates through time utilize multiple measures of productivity, including net primary productivity (e.g., Canfield et al. 2006; Kharecha et al. 2005; Wei et al. 2021; Planavsky et al. 2022); gross primary productivity (e.g., Hodgskiss et al. 2019); and others such as electron-equivalent net primary productivity (e.g., Ward et al. 2018) or gross biosphere production (e.g., Wing 2013). While all these estimates reveal similar trends in productivity through time (as discussed above), export productivity may not always develop in line with primary productivity. Export and primary productivity can indeed be uncoupled through time (e.g., Lopes et al. 2015). An interesting area of future study is how estimates of export productivity through time (such as those implied by our model worlds, Figure 2.4) relate to broader shifts in primary productivity through time.

Supplementary Table 2.1

Group name	Assigned range of appearance in planktic ecosystems (Ma)	Assigned range of maximum size class (μm)	Assigned trophic function
Prokaryotes	3500 to 3200 Stromatolites, isotopic evidence, and probable microfossils suggest the possible presence of life as early as ~3500 Ma, and organic-walled spheroidal microfossils from ~3200 Ma represent some of the best candidates for definitive fossil evidence of early life (Knoll et al. 2016). While much of the evidence of early life is interpreted to come from the benthic realm, Lipps & Culver (2002) hypothesize that both benthic and pelagic ecosystems were widely distributed in Archean seas, with prokaryotic trophic interactions in the open ocean being simpler than modern ones due to smaller plankton sizes, minimal sources of organic debris, and low diversity.	2 to 60 Prokaryotes are generally classified as picoplankton, ranging from 0.2 to 2 μm (Lipps & Culver 2002). A larger maximum size of 60 μm is included here due to the large sizes of the organic-walled spheroidal microfossils ca. ~3200 Ma (ranging from 31 to 298 μm , with a mode between 50 and 75 μm , Javaux et al. 2010), as well as the 10 to 30 μm organic spheroids ca. ~3500, earlier putative microfossils (Knoll et al. 2016). These relatively large microfossils may represent extracellular sheaths, envelopes, or other microstructures that encased early prokaryotes (Javaux et al. 2010; Knoll et al. 2016).	Heterotroph; here we reserve “autotroph” for organisms that fix carbon via oxygenic photosynthesis (see Section 2.2.3 of this paper for a note on terminology).
Cyanobacteria (smaller)	2700 to 1100 The origin of cyanobacteria in the pelagic realm is uncertain; however, Hurley et al. (2021) provide evidence for the presence of pelagic cyanobacteria within the mid-Proterozoic eon, ~1800 to 1000 Ma. Another study using paired biomarker and nitrogen isotope measurements identifies the presence of pelagic cyanobacteria at ~1100 Ma (refs., Hurley et al. 2021). The absolute earliest possible estimates of the origin of pelagic cyanobacteria would overlap with the origin of cyanobacteria, which is shown to have occurred at ~2700 Ma by molecular biomarkers (refs., Katz et al. 2007) and ~2000 Ga by the oldest unambiguous cyanobacterial microfossils found in peritidal black cherts (refs., Hurley et al. 2021).	2 to 3 The upper ranges of modern small cyanobacteria (e.g., <i>Prochlorococcus</i> and <i>Synechococcus</i>) fall around 1 to 2 μm (Bertilsson et al. 2003). A phylogenetic reconstruction posits that cyanobacteria with cell diameters larger than 3 μm did not emerge until after the Great Oxidation Event, and that they emerged later than smaller cyanobacteria (Sánchez-Baracaldo 2015).	Autotroph
Cyanobacteria (larger)	2000 to 1350 Modern large forms of cyanobacteria	15 to 60 <i>Trichodesmium</i> is a large cyanobacteria	Autotroph

Group name	Assigned range of appearance in planktic ecosystems (Ma)	Assigned range of maximum size class (μm)	Assigned trophic function
	<p>such as <i>Trichodesmium</i> indicate a potential range in sizes for cyanobacteria throughout time. According to a phylogenetic reconstruction, larger cyanobacteria above 3 μm did not emerge until after the Great Oxidation Event (Sánchez-Baracaldo 2015), ca. ~2400 to 2000 Ma (refs., Hurley et al. 2021). Additionally, an ancestor of <i>Trichodesmium</i> is estimated to have lived between ~1500 and 1350 Ma, though it is possible this ancestor was benthic (Sánchez-Baracaldo 2015). We continue to follow Hurley et al. (2021)'s finding of the presence of pelagic cyanobacteria in the mid-Proterozoic (ca. ~1800 to 1000 Ma) and allow for the possibility of earlier origins as well.</p>	<p>found in modern oceans, with cell sizes that can range up to 15 μm in diameter and 50 μm in length (Capone et al. 1997). <i>Trichodesmium</i> can form colonies that are ~2 to 5 mm in length or diameter (Capone et al. 1997), though we do not include the upper size limits of these colonies here.</p>	
Eukaryotes (prior to plastid acquisition)	<p>2500 to 1200</p> <p>Crown group eukaryotes could have evolved between 2000 and 1000 Ma, and total-group eukaryotes as early as 3000 Ma, according to molecular clock analyses (refs., Cohen et al. 2021). Plastids were derived after the origin of eukaryotes via an endosymbiotic event with a cyanobacteria (refs., Cohen et al. 2021); <i>Bangiomorpha pubescens</i> (ca. ~1200 to 1100 Ma) is interpreted as part of the Archaeplastida supergroup and supports molecular clock analyses that place the acquisition of plastids (and the last common ancestor of extant eukaryotes) prior to ~1200 Ma (Knoll 2014; Cohen et al. 2021). Finally, though the origins of benthic versus pelagic eukaryotes are uncertain, we follow Lipps & Culver (2002)'s idea that protists likely appeared in pelagic trophic structures beginning in the Paleoproterozoic and Mesoproterozoic (~2500 to 1000 Ma).</p>	<p>10 to 100</p> <p>As fossil evidence for the origin of eukaryotes is lacking (Cohen et al. 2021), a conventional size range for a eukaryotic cell is assigned. This is likely an underestimate (e.g., acritarch fossils from the Proterozoic exceed 100 μm); however, the main purpose here is to represent possible early heterotrophic protists that may have appeared in planktic ecosystems with the origin of eukaryotes. Larger sizes within eukaryotes are represented as part of the acritarchs below, as their fossils provide more specific constraints on possible maximum size.</p>	Heterotroph
Acritarchs (larger)	1800 to 800	100 to 600	Autotroph, as sphaeromorph

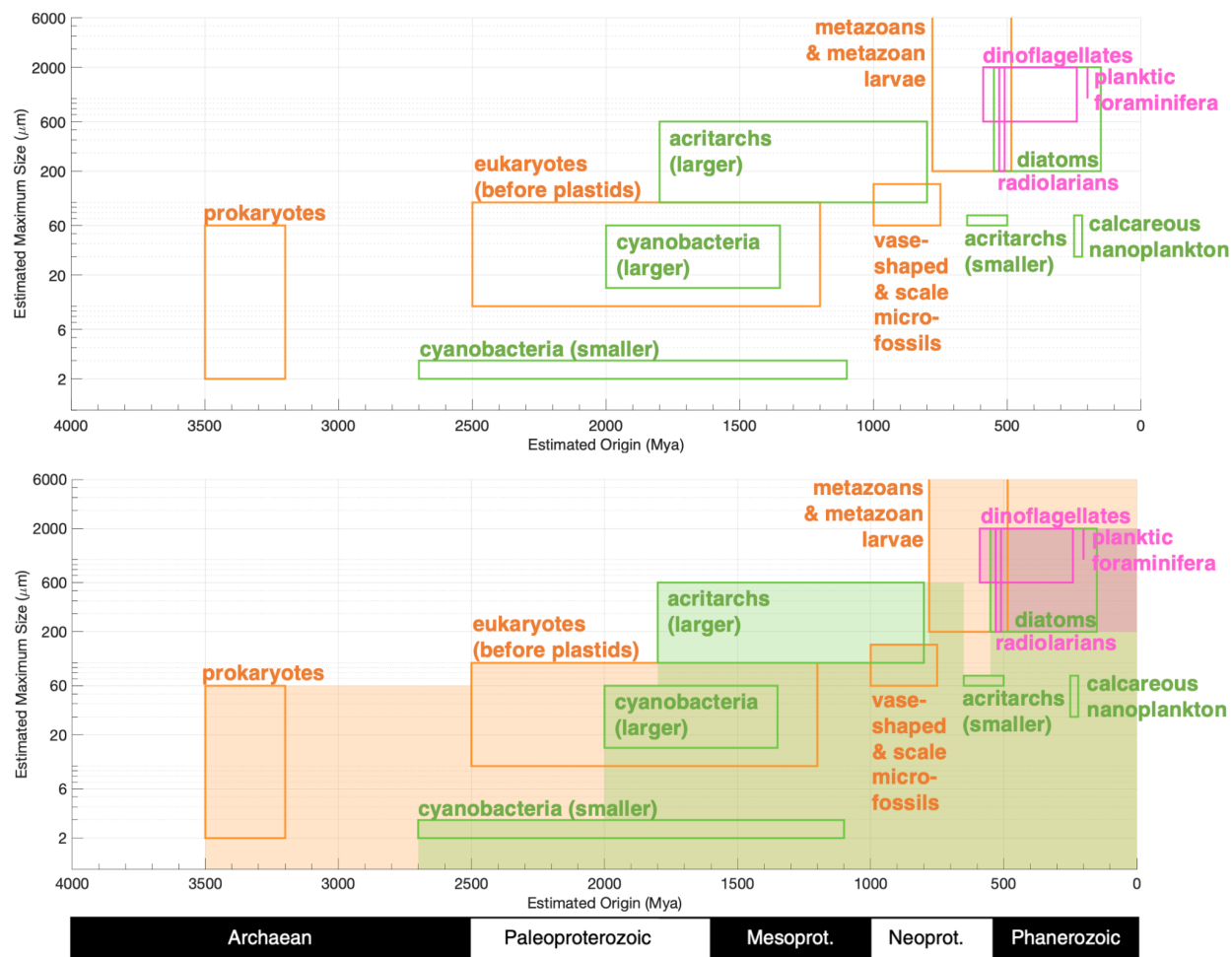
Group name	Assigned range of appearance in planktic ecosystems (Ma)	Assigned range of maximum size class (μm)	Assigned trophic function
	<p>Cohen & Kodner (2021) note that the “first fossils unequivocally identified as total group eukaryotes are acritarchs from ca. 1.7-1.5 Ga.”</p> <p>There is evidence of acritarchs (interpreted as being of red algae lineage) as old as ~1800 Ma, though more definitive evidence exists from ~1200 Ma. There is also evidence of green algae from ~750 to ~800 Mya rocks (Knoll et al. 2007; Knoll et al. 2014). Small spherimorph acritarchs (~100 μm) are generally interpreted as plankton due to their “modest size ... , wide paleoenvironmental range, random bedding-plane distribution, and evident excystment structures” (Butterfield 1997) though there is some uncertainty and doubt regarding larger acritarchs (see right column).</p>	<p>Though sizes can reach 600 μm or higher, Butterfield (1997) cautions against interpreting these as planktic, as there is doubt as to whether or not they could have feasibly stayed in the surface ocean due to their large size and extensive ornamentation.</p>	<p>leipsoparids and acanthromorphic acritarchs are commonly interpreted as phytoplankton (Butterfield 1997; Katz et al. 2007), though their lineage is uncertain.</p>
Acritarchs (smaller)	<p>650 to 500</p> <p>In the Neoproterozoic, a shift in the maximum size of acritarchs occurred. First, small sphaeromorphic acritarchs (<~60 μm) existed from the Paleoproterozoic into the Paleozoic “without significant change” (Butterfield 1997). Second, many acritarch species were lost in an extinction between 650 and 590 Ma (Knoll 1994), and as they re-radiated in the early Cambrian, they were reduced in size (Knoll 1994). The Cambrian acanthromorphs (notable for their large sizes and ornamentation prior to extinction) that re-radiated and persisted throughout the Paleozoic were “fundamentally smaller (typically <75 μm diameter) and much more widely distributed” (Butterfield 1997).</p>	<p>60 to 75</p> <p>See left column.</p>	<p>Autotroph, as sphaeromorph leipsoparids and acanthromorphic acritarchs are commonly interpreted as phytoplankton (Butterfield 1997; Katz et al. 2007), though their lineage is uncertain.</p>
Vase-shaped and scale microfossils	<p>1000 to 750</p> <p>The vase-shaped microfossils and scale microfossils of the Neoproterozoic have uncertain lineage, but have been identified as possibly autotrophic or heterotrophic</p>	<p>60 to 150</p> <p>Cohen & Knoll (2012) estimate that the full organisms represented by scale microfossils (10 to 30 μm) could have been 30 to 140 μm in diameter. Vase-shaped fossils are typically <60 μm</p>	<p>Heterotroph, as these are sometimes interpreted (Butterfield 1997; Knoll 2014; Cohen & Kodner</p>

Group name	Assigned range of appearance in planktic ecosystems (Ma)	Assigned range of maximum size class (μm)	Assigned trophic function
	(Knoll et al. 2014; Cohen & Kodner 2021). Butterfield (1997) identifies vase-shaped microfossils in particular as possible candidates for early microzooplankton.	(Knoll et al. 2014).	2021). They have also been linked to instances of eukaryovory (Knoll 2014; Cohen & Kodner 2021).
Metazoans and metazoan larvae	780 to 485 New molecular clock dates from Erwin (2015) place early metazoan life at ~780 Ma. However it is unclear when metazoans started to inhabit pelagic environments and live planktic lifestyles. Lipps & Culver (2002) hypothesize that microherbivores should have appeared in pelagic trophic structures sometime in the Neoproterozoic, and Butterfield (1997) notes the importance of microzooplankton prior to and at the Proterozoic-Phanerozoic transition. Zhuralev (2015) argues for a late inception of planktic and planktotrophic larvae, either in the middle or end-Cambrian. Thus our most recent estimate for the appearance of metazoan plankton is 485 Ma at the end-Cambrian. There is fossil evidence of a possible filter-feeding brachiopod that may have been some of the first mesozooplankton (Butterfield 1994) and a non-benthic predatory arthropod (Vannier et al. 2009) in the lower and middle Cambrian but again, a planktic life habit is either uncertain (in the case of the former) or unlikely (in the case of the latter).	>200 Metazoans and their larvae encompass a range of sizes. Here we simply set a lower limit and do not define an upper limit. Lipps & Culver (2002) categorize invertebrates and vertebrate larvae as “microplankton,” ranging from 20 to 200 μm , so we take 200 μm as our lower limit.	Heterotroph, though not all planktic larval stages of metazoa are necessarily feeding.
Radiolarians	530 to 510 See Sheng et al. 2020 (and refs.) for middle Cambrian fossil evidence of radiolarians.	200 to 2000 Middle Cambrian radiolarians described in Sheng et al. (2020) range from ~100 to 200 μm ; modern radiolarians can reach 2000 μm or more (www.ucmp.berkeley.edu/protista/radiolaria/rads.html).	Mixotroph
Dinoflagellates	590 to 240	600 to 2000	Mixotroph

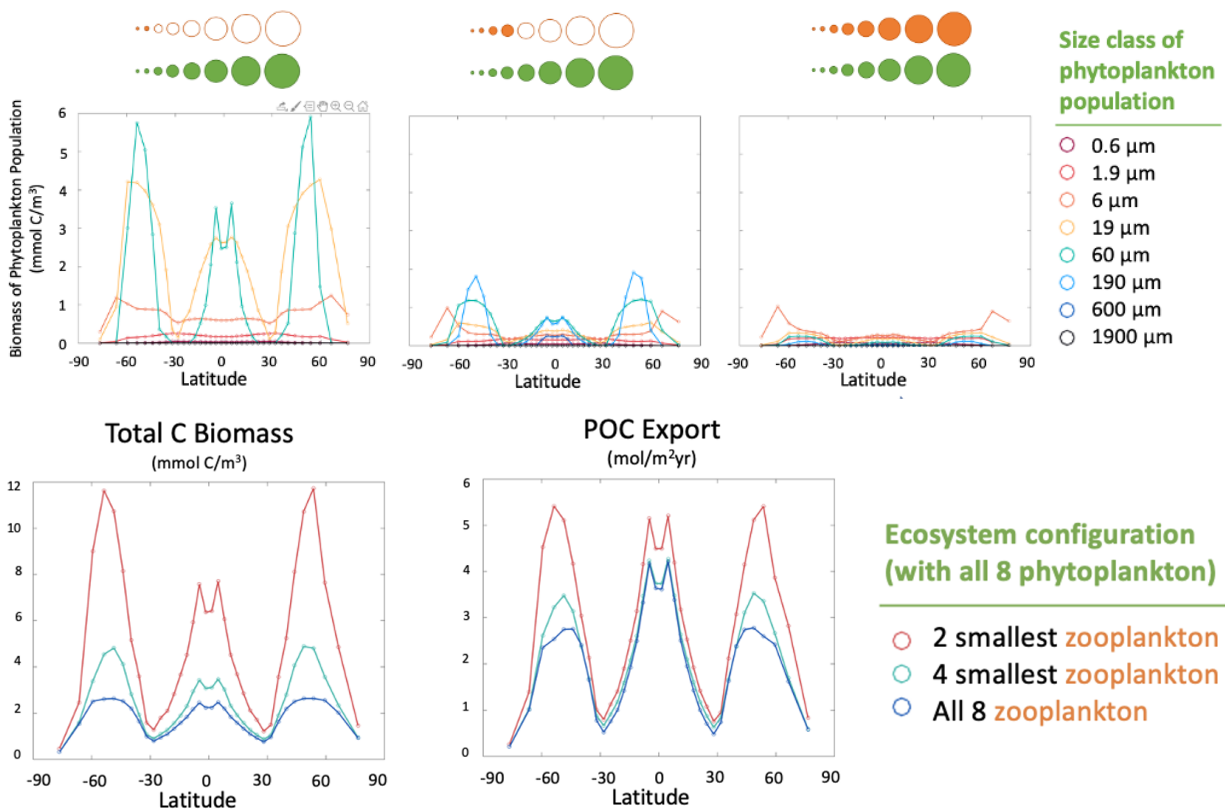
Group name	Assigned range of appearance in planktic ecosystems (Ma)	Assigned range of maximum size class (μm)	Assigned trophic function
	See Katz et al. 2007 and Hull 2017 (and refs.); earlier date comes from biomarker evidence.	Taylor et al. (2008) describe dinoflagellates up to $\sim 600 \mu\text{m}$; some can also reach $2000 \mu\text{m}$ or more (www.britannica.com/science/dinoflagellate).	
Diatoms	550 to 150 See Finkel et al. (2007), Katz et al. (2007), and Hull (2017, and refs.); earlier date comes from biomarker evidence.	200 to 2000 Diatoms typically range from 20 to $200 \mu\text{m}$ in size and can reach $2000 \mu\text{m}$ or more (www.ucl.ac.uk/GeolSci/micropal/diatom.html).	Autotroph, though a few diatoms are obligate heterotrophs.
Calcareous nanoplankton (e.g., coccolithophores)	250 to 220 See Katz et al. (2007) and Hull (2017, and refs.); earlier date comes from biomarker evidence.	30 to 75 Upper ranges in calcareous nanoplankton size of 30 and $75 \mu\text{m}$ are given by Rothwell (2004) and Jordan (2009) respectively.	Autotroph
Planktic foraminifera	200 See Hull 2017 (and refs.).	1000 to 2000 An upper range in planktic foraminifera size of $1000 \mu\text{m}$ is given by Rothwell (2004); additionally, some planktic foraminifera can reach a couple millimeters to centimeters in size.	Mixotroph

Supplementary Table 2.1: References and reasoning for plankton maximum size and origin estimates through time.

Supplementary Figures 2.1 to 2.2



Supplementary Figure 2.1: Contribution of new organismal groups to maximum plankton size over time. Boxes bound the estimated range of origin (box width) and estimated maximum size (box height) of each group. Green indicates “phytoplankton”; orange indicates “zooplankton”; and pink indicates mixotrophic strategies (see Section 2.2.3 for a note on terminology). The color shading in the bottom plot represents the full range of plankton size that may have existed at each point in time, based on the estimated origins and maximum sizes of each plankton group.



Supplementary Figure 2.2: Release from zooplankton grazing drives phytoplankton bloom and high carbon export. The top 3 plots show changes in the biomass of each phytoplankton population as the largest zooplankton populations are eliminated. The bottom 2 plots show how total C biomass and POC export vary as the largest zooplankton populations are eliminated.

Acknowledgements

Unsurprisingly, there are lots of people to thank for this thesis and the fact that I have gotten to study geology/Earth science these past few years. Working on these model worlds (arguably) made me a geology major and my life is fuller because of it. Celli, I have loved being part of the Hull Lab and your constant encouragement, support, and patience as I have hacked away at both understanding and writing up these model worlds have been invaluable. Thank you for taking me in and showing me all the great things about science, the ocean, and paleoecology, AND for all your meticulous edits on this thesis (even at the latest hours!!). Andy, thanks for hosting me those 2 weeks in California and making these model worlds that we get to play with :) and for all your guidance with GENIE, telling me when I've added a bunch of experiments to the wrong queue, and (most importantly) making sure the worlds don't crash. Dominik, thank you for always being so generous with your time even when we have been in very different time zones and for helping me figure out any coding/model/plotting issue I have ever had.

Lots of thanks to professors who I am lucky to have been taught by these past few years—Prof. Evans, you taught my first geo class AND made me go camping for the first time (and it was so fun). Prof. Tarhan, I will always love trace fossils and sedimentary structures because of your class. Plus I am so glad you made us memorize the geologic time scale! Prof. Briggs, I had the best time in history of life lecture in spring 2020 and history of life lab this year! You have introduced me to some of my favorite fossil creatures. Thank you for being my second reader. Noah, thank you for your productivity plot (and all the productivity references) and all your support/patience advising my senior essay for my other major while I have been too fixated on finishing this one.

Everyone in the Hull Lab—thanks for dealing with my messy practice talks 1-2x a year, and then giving me such great, helpful feedback with such care and attention. I will miss seeing you and getting to hear about your cool work every week.

Huge shoutout to my friends who gracefully receive the brunt of all my geology/fossil fun facts I get from class—Blanca, who not only proofread this entire thesis for me and helped me wrangle the references, but lives with me and my antics every day. I will never forget our failed plans for an Ediacaran ocean cake. Cat, for all the lion emojis, post-Climate Change recaps, and text conversations that we seem to always get into when I'm sitting in the lab intending to “do work.” Jean, who is always there to commiserate over research tribulations, since the very beginning in summer 2019. Jisoo, for the company, in real life and virtual, through many late nights writing. Sharon, for listening to me talk productivity plots over avocado toast at brunch. Ellie, who waits for me while I look at all the rocks whenever we go places. Thanks all :)

Endless thanks to my parents and grandparents who have taken me to visit beautiful national parks across the country (and around the world) since I was little, inspired in me a huge appreciation for nature, and supported me through my research and entire time at Yale. I love you!

References

1. Barnosky, A. D., Carrasco, M. A., & Davis, E. B. (2005). The impact of the species–area relationship on estimates of paleodiversity. *PLoS biology*, 3(8), e266.
2. Barton, A. D., Pershing, A. J., Litchman, E., Record, N. R., Edwards, K. F., Finkel, Z. V., ... & Ward, B. A. (2013). The biogeography of marine plankton traits. *Ecology letters*, 16(4), 522-534.
3. Beerling, D. J. (1999). Quantitative estimates of changes in marine and terrestrial primary productivity over the past 300 million years. *Proceedings of the Royal Society of London. Series B: Biological Sciences*, 266(1431), 1821-1827.
4. Bender, M., Sowers, T., & Labeyrie, L. (1994). The Dole effect and its variations during the last 130,000 years as measured in the Vostok ice core. *Global Biogeochemical Cycles*, 8(3), 363-376.
5. Bertilsson, S., Berglund, O., Karl, D. M., & Chisholm, S. W. (2003). Elemental composition of marine Prochlorococcus and Synechococcus: Implications for the ecological stoichiometry of the sea. *Limnology and oceanography*, 48(5), 1721-1731.
6. Boag, T. H., Stockey, R. G., Elder, L. E., Hull, P. M., & Sperling, E. A. (2018). Oxygen, temperature and the deep-marine stenothermal cradle of Ediacaran evolution. *Proceedings of the Royal Society B*, 285(1893), 20181724.
7. Bottjer, D. J. (2016). *Paleoecology: past, present and future*. John Wiley & Sons.
8. Bridgestock, L., Hsieh, Y. T., Porcelli, D., & Henderson, G. M. (2019). Increased export production during recovery from the Paleocene–Eocene thermal maximum constrained by sedimentary Ba isotopes. *Earth and Planetary Science Letters*, 510, 53-63.
9. Bush, A. M., & Payne, J. L. (2021). Biotic and Abiotic Controls on the Phanerozoic History of Marine Animal Biodiversity. *Annual Review of Ecology, Evolution, and Systematics*, 52, 269-289.
10. Butterfield, N. J. (1994). Burgess Shale-type fossils from a Lower Cambrian shallow-shelf sequence in northwestern Canada. *Nature*, 369(6480), 477-479.
11. Butterfield, N. J. (1997). Plankton ecology and the Proterozoic-Phanerozoic transition. *Paleobiology*, 23(2), 247-262.
12. Canfield, D. E., Rosing, M. T., & Bjerrum, C. (2006). Early anaerobic metabolisms. *Philosophical Transactions of the Royal Society B: Biological Sciences*, 361(1474), 1819-1836.
13. Canfield, D. E., Rosing, M. T., & Bjerrum, C. (2006). Early anaerobic metabolisms. *Philosophical Transactions of the Royal Society B: Biological Sciences*, 361(1474), 1819-1836.
14. Capone, D. G., Zehr, J. P., Paerl, H. W., Bergman, B., & Carpenter, E. J. (1997). Trichodesmium, a globally significant marine cyanobacterium. *Science*, 276(5316), 1221-1229.
15. Cohen, P. A., & Knoll, A. H. (2012). Scale microfossils from the mid-neoproterozoic fifteenmile Group, Yukon territory. *Journal of Paleontology*, 86(5), 775-800.
16. Cohen, P. A., & Kodner, R. B. (2021). The earliest history of eukaryotic life: uncovering an evolutionary story through the integration of biological and geological data. *Trends in ecology & evolution*.
17. Cole, Devon B., Kazumi Ozaki, and Christopher T. Reinhard. "Atmospheric oxygen abundance, marine nutrient availability, and organic carbon fluxes to the seafloor." *Earth*

- and Space Science Open Archive ESSOAr* (2021).
18. Connor, E. F., & McCoy, E. D. (1979). The statistics and biology of the species-area relationship. *The American Naturalist*, 113(6), 791-833.
 19. Crichton, K. A., Wilson, J. D., Ridgwell, A., & Pearson, P. N. (2021). Calibration of temperature-dependent ocean microbial processes in the cGENIE. muffin (v0. 9.13) Earth system model. *Geoscientific Model Development*, 14(1), 125-149.
 20. Crockford, P. W., Hayles, J. A., Bao, H., Planavsky, N. J., Bekker, A., Fralick, P. W., ... & Wing, B. A. (2018). Triple oxygen isotope evidence for limited mid-Proterozoic primary productivity. *Nature*, 559(7715), 613-616.
 21. Dahl, T. W., Connelly, J. N., Li, D., Kouchinsky, A., Gill, B. C., Porter, S., ... & Bizzarro, M. (2019). Atmosphere–ocean oxygen and productivity dynamics during early animal radiations. *Proceedings of the National Academy of Sciences*, 116(39), 19352-19361.
 22. Deutsch, C., Ferrel, A., Seibel, B., Pörtner, H. O., & Huey, R. B. (2015). Climate change tightens a metabolic constraint on marine habitats. *Science*, 348(6239), 1132-1135.
 23. Deutsch, C., Penn, J. L., & Seibel, B. (2020). Metabolic trait diversity shapes marine biogeography. *Nature*, 585(7826), 557-562.
 24. Donnadieu, Y., Pucéat, E., Moiroud, M., Guillocheau, F., & Deconinck, J. F. (2016). A better-ventilated ocean triggered by Late Cretaceous changes in continental configuration. *Nature communications*, 7(1), 1-12.
 25. Edwards, C. T., Saltzman, M. R., Royer, D. L., & Fike, D. A. (2017). Oxygenation as a driver of the Great Ordovician Biodiversification Event. *Nature Geoscience*, 10(12), 925-929.
 26. Edwards, K.F., Litchman, E. & Klausmeier, C.A. (2013). Functional traits explain phytoplankton community structure and seasonal dynamics in a marine ecosystem. *Ecol. Lett.*, 16, 56–63.
 27. Edwards, N. R., & Marsh, R. (2005). Uncertainties due to transport-parameter sensitivity in an efficient 3-D ocean-climate model. *Climate dynamics*, 24(4), 415-433.
 28. Erwin, D. H. (2015). Early metazoan life: divergence, environment and ecology. *Philosophical Transactions of the Royal Society B: Biological Sciences*, 370(1684), 20150036.
 29. Falkowski, P.G., Barber, R.T. & Smetacek, V. (1998). Biogeochemical controls and feedbacks on ocean primary production. *Science*, 281, 200–206.
 30. Falkowski, P. G., Laws, E. A., Barber, R. T., & Murray, J. W. (2003). Phytoplankton and their role in primary, new, and export production. In *Ocean biogeochemistry* (pp. 99-121). Springer, Berlin, Heidelberg.
 31. Field, C. B., Behrenfeld, M. J., Randerson, J. T., & Falkowski, P. (1998). Primary production of the biosphere: integrating terrestrial and oceanic components. *science*, 281(5374), 237-240.
 32. Finkel, Z. V. (2007). Does phytoplankton cell size matter? The evolution of modern marine food webs. *Evolution of primary producers in the sea*, 333-350.
 33. Finkel, Z. V., Sebbo, J., Feist-Burkhardt, S., Irwin, A. J., Katz, M. E., Schofield, O. M. E., ... & Falkowski, P. G. (2007). A universal driver of macroevolutionary change in the size of marine phytoplankton over the Cenozoic. *Proceedings of the National Academy of Sciences*, 104(51), 20416-20420.
 34. Flessa, K. W., & Sepkoski, J. J. (1978). On the relationship between Phanerozoic diversity and changes in habitable area. *Paleobiology*, 4(3), 359-366.

35. Follows, M. J., Dutkiewicz, S., Grant, S., & Chisholm, S. W. (2007). Emergent biogeography of microbial communities in a model ocean. *science*, 315(5820), 1843-1846.
36. Friedrich, O., Erbacher, J., Moriya, K., Wilson, P. A., & Kuhnert, H. (2008). Warm saline intermediate waters in the Cretaceous tropical Atlantic Ocean. *Nature Geoscience*, 1(7), 453-457.
37. Gibbs, S. J., Bralower, T. J., Bown, P. R., Zachos, J. C., & Bybell, L. M. (2006). Shelf and open-ocean calcareous phytoplankton assemblages across the Paleocene-Eocene Thermal Maximum: Implications for global productivity gradients. *Geology*, 34(4), 233-236.
38. Gill, B. C., Lyons, T. W., Young, S. A., Kump, L. R., Knoll, A. H., & Saltzman, M. R. (2011). Geochemical evidence for widespread euxinia in the Later Cambrian ocean. *Nature*, 469(7328), 80-83.
39. Grasby, S. E., Beauchamp, B., & Knies, J. (2016). Early Triassic productivity crises delayed recovery from world's worst mass extinction. *Geology*, 44(9), 779-782.
40. Guidi, L., Stemann, L., Jackson, G. A., Ibanez, F., Claustre, H., Legendre, L., ... & Gorsky, G. (2009). Effects of phytoplankton community on production, size, and export of large aggregates: A world-ocean analysis. *Limnology and Oceanography*, 54(6), 1951-1963.
41. Hammarlund, E. U., Gaines, R. R., Prokopenko, M. G., Qi, C., Hou, X. G., & Canfield, D. E. (2017). Early Cambrian oxygen minimum zone-like conditions at Chengjiang. *Earth and Planetary Science Letters*, 475, 160-168.
42. Hodgskiss, M. S., Crockford, P. W., Peng, Y., Wing, B. A., & Horner, T. J. (2019). A productivity collapse to end Earth's Great Oxidation. *Proceedings of the National Academy of Sciences*, 116(35), 17207-17212.
43. Holland, S. M. (2012). Sea level change and the area of shallow-marine habitat: implications for marine biodiversity. *Paleobiology*, 38(2), 205-217.
44. Hull, P. M. (2017). Emergence of modern marine ecosystems. *Current Biology*, 27(11), R466-R469.
45. Hull, P. M., & Norris, R. D. (2011). Diverse patterns of ocean export productivity change across the Cretaceous-Paleogene boundary: New insights from biogenic barium. *Paleoceanography*, 26(3).
46. Hurley, S. J., Wing, B. A., Jasper, C. E., Hill, N. C., & Cameron, J. C. (2021). Carbon isotope evidence for the global physiology of Proterozoic cyanobacteria. *Science advances*, 7(2), eabc8998.
47. Jenkyns, H. C. (2010). Geochemistry of oceanic anoxic events. *Geochemistry, Geophysics, Geosystems*, 11(3).
48. Jetz, W., & Fine, P. V. (2012). Global gradients in vertebrate diversity predicted by historical area-productivity dynamics and contemporary environment. *PLoS biology*, 10(3), e1001292.
49. John, E. H., Wilson, J. D., Pearson, P. N., & Ridgwell, A. (2014). Temperature-dependent remineralization and carbon cycling in the warm Eocene oceans. *Palaeogeography, Palaeoclimatology, Palaeoecology*, 413, 158-166.
50. Jordan, R. W. (2009). Coccolithophores. In M. Schaechter (ed), *Encyclopedia of microbiology*. Academic Press.

51. Katz, M. E., Fennel, K., & Falkowski, P. G. (2007). Geochemical and biological consequences of phytoplankton evolution. In *Evolution of primary producers in the sea* (pp. 405-430). Academic Press.
52. Keeling, R. F., Körtzinger, A., & Gruber, N. (2010). Ocean deoxygenation in a warming world. *Annual review of marine science*, 2, 199-229.
53. Kharecha, P., Kasting, J., & Siefert, J. (2005). A coupled atmosphere–ecosystem model of the early Archean Earth. *Geobiology*, 3(2), 53-76.
54. Knoll, A. H. (1994). Proterozoic and Early Cambrian protists: evidence for accelerating evolutionary tempo. *Proceedings of the National Academy of Sciences*, 91(15), 6743-6750.
55. Knoll, A. H. (2014). Paleobiological perspectives on early eukaryotic evolution. *Cold Spring Harbor Perspectives in Biology*, 6(1), a016121.
56. Knoll, A. H., & Follows, M. J. (2016). A bottom-up perspective on ecosystem change in Mesozoic oceans. *Proceedings of the Royal Society B: Biological Sciences*, 283(1841), 20161755.
57. Knoll, A. H., Summons, R. E., Waldbauer, J. R., & Zumberge, J. E. (2007). The geological succession of primary producers in the oceans. In *Evolution of primary producers in the sea* (pp. 133-163). Academic Press.
58. Knoll, A. H., Bergmann, K. D., & Strauss, J. V. (2016). Life: the first two billion years. *Philosophical Transactions of the Royal Society B: Biological Sciences*, 371(1707), 20150493.
59. Kreft, H., Jetz, W., Mutke, J., Kier, G., & Barthlott, W. (2008). Global diversity of island floras from a macroecological perspective. *Ecology letters*, 11(2), 116-127.
60. Lenton, T. M., Boyle, R. A., Poulton, S. W., Shields-Zhou, G. A., & Butterfield, N. J. (2014). Co-evolution of eukaryotes and ocean oxygenation in the Neoproterozoic era. *Nature Geoscience*, 7(4), 257-265.
61. Lipps, J. H., & Culver, S. J. (2002). The trophic role of marine microorganisms through time. *The Paleontological Society Papers*, 8, 69-92.
62. Liu, P., Liu, J., Ji, A., Reinhard, C. T., Planavsky, N. J., Babikov, D., ... & Kasting, J. F. (2021). Triple oxygen isotope constraints on atmospheric O₂ and biological productivity during the mid-Proterozoic. *Proceedings of the National Academy of Sciences*, 118(51).
63. Lomolino, M. V. (2000). Ecology's most general, yet protean pattern: the species-area relationship. *Journal of Biogeography*, 17-26.
64. Lopes, C., Kucera, M., & Mix, A. C. (2015). Climate change decouples oceanic primary and export productivity and organic carbon burial. *Proceedings of the National Academy of Sciences*, 112(2), 332-335.
65. Lu, W., Ridgwell, A., Thomas, E., Hardisty, D. S., Luo, G., Algeo, T. J., ... & Lu, Z. (2018). Late inception of a resiliently oxygenated upper ocean. *Science*, 361(6398), 174-177.
66. Lyons, T. W., Diamond, C. W., Planavsky, N. J., Reinhard, C. T., & Li, C. (2021). Oxygenation, life, and the planetary system during Earth's middle history: An overview. *Astrobiology*, 21(8), 906-923.
67. MacArthur, R. H., & Wilson, E. O. (1963). An equilibrium theory of insular zoogeography. *Evolution*, 373-387.
68. Marsh, R., Müller, S. A., Yool, A., & Edwards, N. R. (2011). Incorporation of the C-GOLDSTEIN efficient climate model into the GENIE framework:" eb_go_gs"

- configurations of GENIE. *Geoscientific Model Development*, 4(4), 957-992.
69. Meyer, K. M., & Kump, L. R. (2008). Oceanic euxinia in Earth history: causes and consequences. *Annu. Rev. Earth Planet. Sci.*, 36, 251-288.
 70. Meyer, K. M., Yu, M., Jost, A. B., Kelley, B. M., & Payne, J. L. (2011). $\delta^{13}\text{C}$ evidence that high primary productivity delayed recovery from end-Permian mass extinction. *Earth and Planetary Science Letters*, 302(3-4), 378-384
 71. Meyer, K. M., Ridgwell, A., & Payne, J. L. (2016). The influence of the biological pump on ocean chemistry: implications for long-term trends in marine redox chemistry, the global carbon cycle, and marine animal ecosystems. *Geobiology*, 14(3), 207-219.
 72. Norris, R. D., Turner, S. K., Hull, P. M., & Ridgwell, A. (2013). Marine ecosystem responses to Cenozoic global change. *Science*, 341(6145), 492-498.
 73. Payne, J. L., Bachan, A., Heim, N. A., Hull, P. M., & Knope, M. L. (2020). The evolution of complex life and the stabilization of the Earth system. *Interface Focus*, 10(4), 20190106.
 74. Paytan, A., Kastner, M., & Chavez, F. P. (1996). Glacial to interglacial fluctuations in productivity in the equatorial Pacific as indicated by marine barite. *Science*, 274(5291), 1355-1357.
 75. Pietsch, C., & Bottjer, D. J. (2014). The importance of oxygen for the disparate recovery patterns of the benthic macrofauna in the Early Triassic. *Earth-Science Reviews*, 137, 65-84.
 76. Planavsky, N. J., Crowe, S. A., Fakhraee, M., Beaty, B., Reinhard, C. T., Mills, B. J., ... & Konhauser, K. O. (2021). Evolution of the structure and impact of Earth's biosphere. *Nature Reviews Earth & Environment*, 2(2), 123-139.
 77. Planavsky, N. J., Fakhraee, M., Bolton, E. W., Reinhard, C. T., Isson, T. T., Zhang, S., & Mills, B. J. W. (2022). On carbon burial and net primary production through Earth's history. *American Journal of Science* (forthcoming).
 78. Preston, F. W. (1962). The canonical distribution of commonness and rarity: Part I. *Ecology*, 43(2), 185-215.
 79. Raup, D. M. (1976). Species diversity in the Phanerozoic: an interpretation. *Paleobiology*, 2(4), 289-297.
 80. Reinhard, C. T., & Planavsky, N. J. (2021). The History of Ocean Oxygenation. *Annual review of marine science*, 14.
 81. Reinhard, C. T., Planavsky, N. J., Ward, B. A., Love, G. D., Le Hir, G., & Ridgwell, A. (2020). The impact of marine nutrient abundance on early eukaryotic ecosystems. *Geobiology*, 18(2), 139-151.
 82. Ridgwell, A., & Schmidt, D. N. (2010). Past constraints on the vulnerability of marine calcifiers to massive carbon dioxide release. *Nature Geoscience*, 3(3), 196-200.
 83. Ridgwell, A., Hargreaves, J. C., Edwards, N. R., Annan, J. D., Lenton, T. M., Marsh, R., ... & Watson, A. (2007). Marine geochemical data assimilation in an efficient Earth System Model of global biogeochemical cycling. *Biogeosciences*, 4(1), 87-104.
 84. Rigby, S., & Milsom, C. V. (2000). Origins, evolution, and diversification of zooplankton. *Annual Review of Ecology and Systematics*, 31(1), 293-313.
 85. Rosenberg, Y. O., Ashckenazi-Polivoda, S., Abramovich, S., Thibault, N., Chin, S., Feinstein, S., ... & Amrani, A. (2021). Resilience of primary and export productivity in a

- eutrophic ecosystem following the Cretaceous-Paleogene mass extinction. *Global and Planetary Change*, 196, 103371.
86. Rothwell, R. G. (2004). Deep ocean pelagic oozes. Vol. 5. of Selley. *Encyclopedia of Geology*. Elsevier, Oxford.
 87. Sánchez-Baracaldo, P. (2015). Origin of marine planktonic cyanobacteria. *Scientific reports*, 5(1), 1-10.
 88. Sepkoski, J. J. (1976). Species diversity in the Phanerozoic: species-area effects. *Paleobiology*, 2(4), 298-303.
 89. Sepkoski, J. J. (1997). Biodiversity: past, present, and future. *Journal of Paleontology*, 71(4), 533-539.
 90. Sepúlveda, J., Wendler, J. E., Summons, R. E., & Hinrichs, K. U. (2009). Rapid resurgence of marine productivity after the Cretaceous-Paleogene mass extinction. *Science*, 326(5949), 129-132.
 91. Shaw, J. O., Briggs, D. E., & Hull, P. M. (2021). Fossilization potential of marine assemblages and environments. *Geology*, 49(3), 258-262.
 92. Shen, J., Zhou, L., Feng, Q., Zhang, M., Lei, Y., Zhang, N., ... & Gu, S. (2014). Paleo-productivity evolution across the Permian-Triassic boundary and quantitative calculation of primary productivity of black rock series from the Dalong Formation, South China. *Science China Earth Sciences*, 57(7), 1583-1594.
 93. Sheng, J., Kachovich, S., & Aitchison, J. C. (2020). Skeletal architecture of middle Cambrian spicular radiolarians revealed using micro-CT. *Journal of Micropalaeontology*, 39(1), 61-76.
 94. Sperling, E. A., Frieder, C. A., Raman, A. V., Girguis, P. R., Levin, L. A., & Knoll, A. H. (2013). Oxygen, ecology, and the Cambrian radiation of animals. *Proceedings of the National Academy of Sciences*, 110(33), 13446-13451.
 95. Sperling, E. A., Knoll, A. H., & Girguis, P. R. (2015). The ecological physiology of Earth's second oxygen revolution. *Annual Review of Ecology, Evolution, and Systematics*, 46, 215-235.
 96. Stockey, R. G., Pohl, A., Ridgwell, A., Finnegan, S., & Sperling, E. A. (2021). Decreasing Phanerozoic extinction intensity as a consequence of Earth surface oxygenation and metazoan ecophysiology. *Proceedings of the National Academy of Sciences*, 118(41).
 97. Stoll, H. M., Shimizu, N., Archer, D., & Ziveri, P. (2007). Coccolithophore productivity response to greenhouse event of the Paleocene–Eocene Thermal Maximum. *Earth and Planetary Science Letters*, 258(1-2), 192-206.
 98. Taylor, F. J. R., Hoppenrath, M., & Saldarriaga, J. F. (2008). Dinoflagellate diversity and distribution. *Biodiversity and conservation*, 17(2), 407-418.
 99. Tittensor, D. P., Mora, C., Jetz, W., Lotze, H. K., Ricard, D., Berghe, E. V., & Worm, B. (2010). Global patterns and predictors of marine biodiversity across taxa. *Nature*, 466(7310), 1098-1101.
 100. Torfstein, A., Winckler, G., & Tripathi, A. (2010). Productivity feedback did not terminate the Paleocene-Eocene Thermal Maximum (PETM). *Climate of the Past*, 6(2), 265-272.
 101. Valentine, J. W., & Jablonski, D. (1991). Biotic effects of sea level change: the

- Pleistocene test. *Journal of Geophysical Research: Solid Earth*, 96(B4), 6873-6878
102. Valentine, J. W., & Moores, E. M. (1970). Plate-tectonic regulation of faunal diversity and sea level: a model. *Nature*, 228(5272), 657-659
 103. Vannier, J., García-Bellido, D. C., Hu, S. X., & Chen, A. L. (2009). Arthropod visual predators in the early pelagic ecosystem: evidence from the Burgess Shale and Chengjiang biotas. *Proceedings of the Royal Society B: Biological Sciences*, 276(1667), 2567-2574.
 104. Wang, X., Cawood, P. A., Zhao, L., Chen, Z. Q., Zhang, L., Lyu, Z., & Ye, F. (2021). Marine productivity variations and environmental perturbations across the early Triassic Smithian-Spathian boundary: Insights from zinc and carbon isotopes. *Global and Planetary Change*, 205, 103579.
 105. Ward, B. A., & Follows, M. J. (2016). Marine mixotrophy increases trophic transfer efficiency, mean organism size, and vertical carbon flux. *Proceedings of the National Academy of Sciences*, 113(11), 2958-2963.
 106. Ward, B. A., Wilson, J. D., Death, R. M., Monteiro, F. M., Yool, A., & Ridgwell, A. (2018). EcoGENIE 1.0: plankton ecology in the cGENIE Earth system model. *Geoscientific Model Development*, 11(10), 4241-4267.
 107. Ward, L. M., Rasmussen, B., & Fischer, W. W. (2019). Primary productivity was limited by electron donors prior to the advent of oxygenic photosynthesis. *Journal of Geophysical Research: Biogeosciences*, 124(2), 211-226.
 108. Wei, G. Y., Planavsky, N. J., He, T., Zhang, F., Stockey, R. G., Cole, D. B., ... & Ling, H. F. (2021). Global marine redox evolution from the late Neoproterozoic to the early Paleozoic constrained by the integration of Mo and U isotope records. *Earth-Science Reviews*, 214, 103506.
 109. Williams, C. B. (1943). Area and number of species. *Nature*, 152(3853), 264-267.
 110. Wilson, J. D., Monteiro, F. M., Schmidt, D. N., Ward, B. A., & Ridgwell, A. (2018). Linking marine plankton ecosystems and climate: a new modeling approach to the warm early Eocene climate. *Paleoceanography and Paleoclimatology*, 33(12), 1439-1452.
 111. Wing, B. A. (2013). A cold, hard look at ancient oxygen. *Proceedings of the National Academy of Sciences*, 110(36), 14514-14515.
 112. Winguth, A. M., Thomas, E., & Winguth, C. (2012). Global decline in ocean ventilation, oxygenation, and productivity during the Paleocene-Eocene Thermal Maximum: Implications for the benthic extinction. *Geology*, 40(3), 263-266.
 113. Zachos, J. C., Arthur, M. A., & Dean, W. E. (1989). Geochemical evidence for suppression of pelagic marine productivity at the Cretaceous/Tertiary boundary. *Nature*, 337(6202), 61-64.
 114. Zaffos, A., Finnegan, S., & Peters, S. E. (2017). Plate tectonic regulation of global marine animal diversity. *Proceedings of the National Academy of Sciences*, 114(22), 5653-5658.
 115. Zhuravlev, A. Y. (2015). The early history of the Metazoa—a paleontologist's viewpoint. *Biology Bulletin Reviews*, 5(5), 415-461.